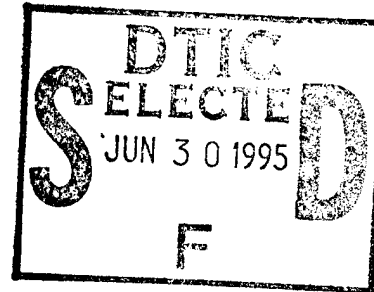


PL-TR-94-2214

**INVESTIGATION OF UPPER MANTLE  
STRUCTURE IN CENTRAL EURASIA FROM  
ANALYSIS OF BROAD-BAND FAR REGIONAL  
SEISMOGRAMS (AND COMPARISON TO  
WESTERN U.S.)**

Karl Koch



Southern Methodist University  
Dallas, TX 75275

July 1994

Final Report  
15 July 1991 - 30 July 1994

Approved for public release; distribution unlimited

DTIC QUALITY INSPECTED 5



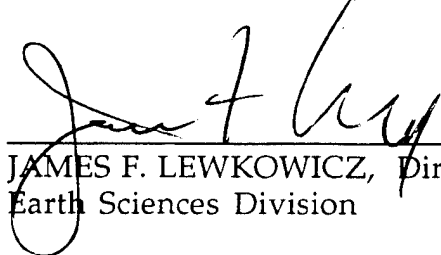
PHILLIPS LABORATORY  
Directorate of Geophysics  
AIR FORCE MATERIEL COMMAND  
HANSCOM AIR FORCE BASE, MA 01731-3010

19950629 036

The views and conclusions contained in this document are those of the authors and should not be interpreted as representing the official policies, either express or implied, of the Air Force or the U.S. Government.

This technical report has been reviewed and is approved for publication.

  
\_\_\_\_\_  
JAMES F. LEWKOWICZ  
Contract Manager  
Earth Sciences Division

  
\_\_\_\_\_  
JAMES F. LEWKOWICZ, Director  
Earth Sciences Division

This report has been reviewed by the ESC Public Affairs Office (PA) and is releasable to the National Technical Information Service (NTIS).

Qualified requestors may obtain additional copies from the Defense Technical Information Center. All others should apply to the National Technical Information Service.

If your address has changed, or if you wish to be removed from the mailing list, or if the addressee is no longer employed by your organization, please notify PL/TSI, 29 Randolph Road, Hanscom AFB, MA 01731-3010. This will assist us in maintaining a current mailing list.

Do not return copies of this report unless contractual obligations or notices on a specific document requires that it be returned.

# REPORT DOCUMENTATION PAGE

Form Approved  
OMB No. 0704-0188

Public reporting burden for this collection of information is estimated to average 1 hour per response, including the time for reviewing instructions, searching existing data sources, gathering and maintaining the data needed, and completing and reviewing the collection of information. Send comments regarding this burden estimate or any other aspect of this collection of information, including suggestions for reducing this burden, to Washington Headquarters Services, Directorate for Information Operations and Reports, 1215 Jefferson Davis Highway, Suite 1204, Arlington, VA 22202-4302, and to the Office of Management and Budget, Paperwork Reduction Project (0704-0188), Washington, DC 20503.

1. AGENCY USE ONLY (Leave blank)		2. REPORT DATE July 1994	3. REPORT TYPE AND DATES COVERED Final 7/15/91 - 7/30/94	
4. TITLE AND SUBTITLE Investigation of Upper Mantle Structure in Central Eurasia From Analysis of Broad-Band Far Regional Seismograms (and Comparison to Western U.S.)			5. FUNDING NUMBERS PE 69120C PR T121 TA TC WU AA	
6. AUTHOR(S)  Karl Koch			Contract F19628-91-K-0016	
7. PERFORMING ORGANIZATION NAME(S) AND ADDRESS(ES)  Southern Methodist University Dallas, TX 75275			8. PERFORMING ORGANIZATION REPORT NUMBER	
9. SPONSORING/MONITORING AGENCY NAME(S) AND ADDRESS(ES)  Phillips Laboratory 29 Randolph Road Hanscom AFB, MA 01731-3010  Contract Manager: James Lewkowicz/GPE			10. SPONSORING/MONITORING AGENCY REPORT NUMBER  PL-TR-94-2214	
11. SUPPLEMENTARY NOTES				
12a. DISTRIBUTION / AVAILABILITY STATEMENT  Approved for public release; distribution unlimited			12b. DISTRIBUTION CODE	
13. ABSTRACT (Maximum 200 words)  Waveforms from nuclear explosions at the E. Kazakhstan test site were recorded at ARU & GAR at the distance range studied for Nevada Test Site explosions (between 1380 and 1540 km). Waveforms at ARU are characterized by weak initial P waves following by strong secondary arrivals within 5 seconds. Within approximately 14 seconds comes a strong later arrival, preceded by a longer-period arrival. Filtering in different frequency bands shows initial P wave & long period arrival are consistent with an amplitude ratio of 1:2. Other arrivals are high-frequency & vanish for periods longer than 2 sec. Synthetic reflectivity seismogram calculations test previous P wave models for Central Eurasia for compatibility with identified waveform patterns. Most models produce impulsive 1st arrivals & fail to generate strong secondary arrivals. Only models by Mechie et al. (1993) & Priestley & Cipar (1994) show some observed P wave patterns. With a new model strong secondary arrivals are generated with observed frequencies & attribute these arrivals to a Moho underside reflection & free surface reflection PP. Complete seismogram calculations indicate a positive gradient below the Moho is needed to match increasing S wave amplitudes observed at ARU between initial S arrival & Lg.				
14. SUBJECT TERMS  Waveforms, synthetic reflectivity, synthetic seismogram modeling, P wave seismograms			15. NUMBER OF PAGES 44	
17. SECURITY CLASSIFICATION OF REPORT Unclassified			16. PRICE CODE	
18. SECURITY CLASSIFICATION OF THIS PAGE Unclassified		19. SECURITY CLASSIFICATION OF ABSTRACT Unclassified		20. LIMITATION OF ABSTRACT SAR

## Introduction

Investigations of the upper mantle structure in Central Eurasia can be considered as a two-tier approach. On the one hand the upper mantle has been probed with short- and long-period P wave seismograms including the studies by King & Calcagnile (1976) and Given and Helmberger (1980), who both used P waves from nuclear explosions in the former Soviet Union recorded at western and northern European seismic stations to investigate the upper mantle P wave structure. While King & Calcagnile's (1976) work was solely based on travel time curves and slowness estimations, Given & Helmberger (1980) used synthetic seismogram calculations to aid in the interpretation of the observations. Both models included a moderate velocity gradient below the Moho (crustal thickness 40 km) to depths of 200 and 160 km, respectively, below which they differed significantly. The KCA model (King & Calcagnile, 1976) included decreasing gradients below 200 km with a velocity increase of 7% across the 420 km discontinuity, while the K8 model (Given & Helmberger, 1980) featured a low velocity zone below 160 km with moderate gradients to 420 km where a smaller velocity contrast of only 4.5% was required. In a similar study more recently, Goldstein et al. (1992) studied wave propagation at regional distances using nuclear explosions at the East Kazakhstan test site as source array in order to estimate slowness at the IRIS stations Arti (ARU), Garm (GAR) and Obninsk (OBN) for a series of 2-4 pulses they detected within the early P wave seismograms. In their subsequent analysis and synthetic seismogram modeling they argued for two competing models with either a discontinuity near 220 km or a notch-shaped low-velocity zone between 100 and 140 km in order to match early arrivals while the discontinuity near 420 km included a 6.5% velocity increase.

For the second approach of estimating upper mantle velocity structure, several studies during the last decade are based on long-range deep seismic sounding (DSS) experiments conducted in the former Soviet Union starting in the early 1970's (e.g. Yegorkin & Pavlenkova, 1981; Vinnik & Ryaboy, 1981, Pavlenkova & Yegorkin, 1983; Mechie et al., 1993, Priestley & Cipar, 1994). For these profiles, which reached distance ranges of up to 4000 km, peaceful nuclear explosions (PNE's) were used providing the necessary seismic energy to be observed at these large offsets from the source. These DSS profiles are shown in Fig.1 along with tectonic features for the Eurasian region and were extensively described by Benz et al. (1992).

<input checked="" type="checkbox"/>	
<input type="checkbox"/>	
<input type="checkbox"/>	
	ies
	or
Dist	Special
A-1	

Seismogram sections from the DSS profiles are typically characterized (e.g. Vinnik & Ryaboy, 1981; Mechie et al., 1993; Priestley & Cipar, 1994) by observations of Pg to distances of 200 km as first arrivals and 500-600 km as secondary arrivals. Pn and mantle P waves are observed from 200 km with apparent phase velocities between 8.2 and 8.5 and are particularly strong in amplitude between about 600-1200 km. Beyond about 1300 km, the first arriving P wave is often quite emergent and is consistently followed by a secondary arrival that can be identified at distances of 900-1000 km with fairly strong amplitudes. Reflections from the 420 km discontinuity are usually identified beyond 1500 km and the forward branch for the refraction below the discontinuity becomes the first arrival at distances of 2000-2200 km. Although not relevant for the scope of this study, the long-range DSS profiles also show the refraction from the 670 km discontinuity becoming the first arrival beyond 2700-2800 km while the reflection can be identified at distances as close as 2200 km.

In this study, we want to take advantage of this previous work and compare synthetic seismogram calculations for various one-dimensional models with the deep seismic sounding results as well as single station observations at station Arti (ARU) and Garm (GAR). First we will characterize the observed wavefield, including identification of the early P wave arrivals mentioned by Goldstein et al. (1992) and mantle S wave arrivals. In addition we will compare these central Eurasian data from a stable continental platform with nuclear explosion data from the tectonic western North America, as station LTX in Texas is at a similar range from the Nevada Test Site as ARU and GAR from the East Kazakhstan site. The next step will include the modeling of P waves between 800 and 1800 km distance with important implications for the velocity distribution of the upper 200 km depth range from the relative amplitudes of relevant upper mantle phases. In the last part we want to investigate the observed S wave pattern, especially the mantle S waves that are well developed in the ARU observations even from isotropic explosion sources. Particular attention in this respect will be paid to the Lg phase which is quite impulsive and shows velocities between 3.6-3.7 km/sec.

## Data analysis

In this study we analyze complete far-regional seismograms from explosions at the Soviet test site in East Kazakhstan including the event from the joint verification experiment to investigate upper mantle structure in Central Eurasia. The data were recorded at the IRIS stations Arti (ARU) and Garm (GAR) with broad-band sensors consisting of Guralp CGM-3 and Streckeisen STS-1 seismometers. These data were previously studied and the P wave part was investigated for upper mantle P wave structure by Goldstein et al. (1992). The purpose of this study is two-fold: (1) reexamine the P waves and compare the observations with synthetic seismograms calculated for new models that were established from deep seismic sounding (DSS) profiles published in recent years (i.e. Mechie et al., 1993, Priestley & Cipar, 1994); (2) to model the S wave part, in particular mantle S waves and the Lg phase, which is often used for yield estimation or in discrimination work.

The station location and the event location are sketched in Fig.1 and the event parameters are summarized in Tab.1. The path from East Kazakhstan to ARU with lengths of 1490-1540 km is almost entirely within the West Siberian platform and is almost alongside the DSS profile #43 which was carried out in 1988, however, to the knowledge of the author there exist no published results so far from this experiment. Results from the closest DSS profile (#32), which was almost exactly 1000 km to the east along similar strike and with similar path length within the West Siberian platform (applying for the southernmost shot point), were reported by Mechie et al. (1993). A second DSS profile (#25) 800 km farther to the east was recently studied by Priestley & Cipar (1994). The experiment on profile #45 was conducted in 1989 (Ryberg, 1993) and is closest to the path to GAR, but here also no results have been published yet.

Vertical and radial component seismograms at ARU are shown in Figs.2a,b. Traces are aligned on the first P wave arrival starting after 20 s into the trace. Except for the first two traces with large microseismic background noise, where event magnitudes are less or equal 5, event to event variations are fairly small. The traces are characterized by a P wave with an emergent first arrival followed by a secondary pulse comprising maximum P wave amplitudes. Secondary arrivals are attributed to S mantle waves starting at about 170 sec into the trace and the Lg wave which arrives about 270 sec into the trace. From the P travel time of 190-195 sec, the Lg waves phase velocity is thus nearly 3.5 km/sec.

Enlarging the P wave portion and filtering the data as shown in Figs.3 shows that the initial emergent P wave is long-period and is followed by higher frequency arrivals arriving between 2 and 5 sec later. Another high-frequency arrival with the highest P wave amplitudes arrives 13-14 sec after the initial P wave. Also a notable low-frequency swing precedes this arrival. Goldstein et al. (1992) identified 4 different arrivals within this P wave packet, attributing the first arrival to a shallow direct wave and the later higher frequency phases to reflections off deeper discontinuities. Filtering the data in the pass-band of 1-5 sec (Fig.3b) shows the first arrival enhanced in amplitude, as well as the low frequency arrival preceding the last high-frequency arrival. Remarkable is the apparent constant amplitude ratio between these two pulses of 1:2, in both the broad-band as well as this longer period band, and the disappearance of the late high-frequency arrival representing the maximum amplitude in the raw data. This high-amplitude, high-frequency arrival was interpreted by Goldstein et al. (1992) as the reflection from the 400 km discontinuity, while this work argues for the lower frequency and earlier arrival to be this reflection. If deeper penetrating rays are consistent with longer period arrivals, this waveform pattern further argues, that the secondary high-frequency energy most likely propagates shallower in the upper mantle contrary to the assumption of Goldstein et al. (1992).

In Fig.3c the P wave portion was further examined by passing the broadband vertical data through different zero phase Butterworth band passes with a total of 4 poles and with the lower corner frequency fixed at 33 sec. Except for the last trace with upper corner at 4 sec where the microseismic noise is significant, all traces show a constant amplitude ratio of 1:2 between the initial P arrival and the longer period later arrival. Interesting furthermore is the fact that the energy following the first arrival and the longer period secondary arrival are only observed for frequencies higher than 1 Hz. In contrast to Goldstein et al. (1992) we consider therefore these arrivals as narrow-band between about 1-3 Hz (the high-frequencies were shown by Goldstein et al. (1992) to disappear above 3 Hz), while the other arrivals are quite broad-band extending from a few seconds to a few Hertz.

In Fig.4a the S wave portion is shown with indication for a mantle S arrival at about 150 sec after the first arriving P (170 sec into the trace). In addition a secondary arrival is also identified with a delay of about 17-18 sec. Both arrivals can be interpreted as the direct mantle S arrival generated from the free surface conversion

at the source and the S wave reflection from the 400 km discontinuity. Further energy can be correlated with a delay of 30 sec with respect to the first mantle S arrival, and it might be speculated this to be the free surface reflection SS similar to the pattern within the P waves. It should be noted that if the data are filtered with lower frequencies, these arrivals become more intermittent, thus 0.2-0.6 Hz appears to be the optimum frequency band for the shear wave energy. Surface waves, shown for period between 10 and 50 secs in Fig.4b, are arriving between 300-350 sec after the P wave and hence have group velocities near 3.0 km/sec. A multiple filter analysis (Dziewonski et al., 1969) of the data suggests a Airy phase with frequencies near 20 sec similar to the Rg phase with a group velocity minimum of 3.0 km/sec.

#### Comparison with Western U.S. far-regional explosion data

In Figs.5 we contrast regional seismograms from both Joint Verification Experiment (JVE) explosions detonated at the Nevada Test Site on Aug. 17, 1988 and at the Soviet test site in East Kazakhstan on Sep.14, 1988 which were observed at similar ranges from the source. Station LTX is at an epicentral distance of 1468 km from the NTS source, while stations GAR and ARU are located 1386 km and 1530 km, respectively, from the East Kazakhstan site. In both regions the P wave at these distances is characterized by the direct mantle P wave and the 400 km reflection. This pattern is further enhanced by the low-pass filtered P waves shown in Fig.5b which also indicates that there is a significant drop of amplitudes for the reflection at GAR. On the other hand the Lg appears quite similar although slightly slower for the western U.S. Both the apparent longer periods observed throughout the seismogram and the much higher signal for the surface wave at LTX indicate the stronger attenuation of high frequency body waves and associated scattered waves.

Filtering the P waves in different frequency bands as carried out for the records displayed in Fig.5c shows a similar pattern for the Western U.S as was demonstrated for Central Eurasia. While the initial P wave and the 400 km reflection are emphasized by the low-passed records, it is obvious that especially Pn (or the wave guided in the mantle lid (Koch & Stump, 1993; Burdick & Helmberger, 1978)) and some later phases are much higher frequency and compare with the higher frequencies observed for later phases at ARU. Therefore it is suggested that higher frequency energy does not penetrate as deep into the mantle than direct P or the 400 km reflection.



### Synthetic seismogram modeling

In the preceding section the waveform characteristics in particular of the P waves as well as the complete far-regional seismograms were extensively discussed. In this section we use synthetic seismogram modeling in order to investigate various proposed velocity models for Central Eurasia for their ability of reproducing the waveforms observed at ARU (or GAR) including models derived from previous seismogram modeling (Fig. 6a) and more recently published models from interpretation of DSS profiles mainly on the Siberian platform (Fig.6b). For the waveform modeling we used the extended reflectivity method (e.g. Müller, 1985), which only accounts for a one-dimensional velocity structure, but which was also applied in many previous studies (i.e. Goldstein et al, 1992; Mechie et al., 1993; Priestley & Cipar, 1994). For all calculations a consistent set of parameters was used: a source depth of 500 m, although Ryberg (1993) mentions a typical emplacement depth of about 800 m for most of the nuclear devices used in the PNE experiments; a source duration of 1 sec applying a Bruestle-Müller source function (Bruestle & Müller, 1983) except for the cases where a different source duration is explicitly mentioned, and an acausal, frequency-independent attenuation model adopted after Der et al (1986) including  $Q_p$  of 900 in the crust, about 600 in a depth range of 100 km below the Moho and 400 for depths to the upper mantle transition zone. The attenuation value for S waves in each layer was chosen according to the relation  $Q_p/Q_s=9/4$ . Different frequency and slowness parameters were used depending on only P wave calculations or calculations of the entire seismograms within reasonable computation times and are described in the appropriate sections.

The stable continental shield (Central Eurasia/ Canada) models shown in Figure 6a were derived from travel-times/ slowness analysis and/or waveform modeling and are consistent (with the exception of Goldstein et al., 1992) in that they show moderate gradients for the upper 200 km in the P wave velocities with reduced gradients above the 400 km discontinuity. Only Given & Helmberger's K8 model and Goldstein et al.'s models include a low velocity zone above 200 km which was also speculated about by Vinnik & Ryaboy (1981). All models have similar 400 and 700 km discontinuities both in velocity contrast and depth as well as the gradient in the transition zone. Models from deep-seismic sounding (Fig.6b) also show quite strong similarities, as most include small to moderate gradients to depths of about 120 km although the associated velocities extend over a significant range, with a strong increase in the gradient within a depth interval of a few to a few tens of

kilometers near this depth, underlain by a depth region with notches of higher and lower velocities. There is also considerable variation among the models for the upper mantle discontinuities near 400 and 700 km, reflecting the ranges at which these reflections were observed as well as their amplitudes on the different profile lines. In the first part of this section these models which were developed purely from P wave observations are revisited to investigate their appropriateness for modeling the P wave observations at ARU. Although some of the models were also used by Goldstein et al. (1992), the newer models from DSS profiling were not available at that time.

#### a) P wave seismograms

For the synthetic P wave seismograms we chose phase velocity integration limits of 7.8 and 20 km/s in order to include all upper mantle P phases but eliminating possible later phases such as Pg as the total length of the time window of 51.2 sec would cause otherwise well-known wrap-around effects. All frequencies from 0.05 to 4 Hz were included. In Figs.7 we summarize the results from the reflectivity method for the various published models for Central Eurasia for the distance range from 800-1800 km. Model KCA shown in Fig.7a is characterized by the direct P arrival turning above 200 km in the upper mantle and the reflection from the 400 km discontinuity as the strongest arrivals in this time window. Secondary arrivals are crustal multiples from the direct P (both the first crustal multiple and the PP phase which arrive at nearly the same time) as well as S-P converted multiples (the phase preceding the PP arrival is the surface converted S-P arrival, where the path from the surface to the Moho is of S type - the phase trailing the PP reflection is the multiple corresponding to PP with one leg in the crust a S wave). At distances larger than 1200-1300 km the initial P wave arrival is followed by a low-amplitude later arrival that can be attributed to the Moho underside reflection. Both the reversed amplitude ratio for the main phases as well as the lack of later arriving energy were considered by Goldstein et al. (1992) as a reason to reject this model as well as model K8 (Given & Helmberger, 1980) considering them inappropriate for the observations at ARU. Model K8 (Fig.7b) and S25 (Fig.7c), which was developed for path within the Canadian shield region, show similar patterns as KCA with the exception of somewhat stronger amplitudes for the 400 km reflection and a reduced amplitude for the initial P wave for distances greater than 1600 and 1700 km, respectively, due to the low velocity zones in these models below 140 and 165 km,

respectively. The fourth of the models derived mainly from traveltime analysis and waveform modeling is CE200 (Goldstein et al., 1992) and its corresponding synthetic seismograms are displayed in Fig.7d. The model calculations show a very strong reflection from a discontinuity located at 200 km depth as well as from the 400 km discontinuity. The broad-band seismograms in the 1500-1600 km distance range confirm the amplitude ratios as observed by Goldstein in the 0.5-1.5 Hz frequency band. Their alternative model CELVZ produces a similar result when looking into the distances appropriate for ARU, with strong reflections for distances between 900 and 1300 km and an even smaller initial P wave.

A second set of synthetic seismograms for models derived from the interpretation of DSS data is shown in Fig.7e-h. The model found by Vinnik & Ryaboy (1981) for seismic observations along a long-range profile on the East-European platform shows a relatively similar waveform pattern as previous models with a fairly impulsive first arrival and a strong reflection from a discontinuity near 400 km depth. However a few noteworthy differences are the increased amplitudes for the crustal multiples and conversions and the secondary phase that is observed beyond 1200 km. For the remaining three models by Mechie et al (1993), shown in Fig.7f (Quartz-N) and Fig.7h (Quartz-S), and by Priestley & Cipar (1994) in Fig.7g, all predict small amplitudes for the reflection near 400 km for distances less than applicable for ARU. However these models (see Fig.6b) are quite similar in the predicted P waveforms, although the profile lines are some 1000 km apart and are confined to different tectonic units such as the West Siberian basin and the Siberian platform. First, they predict quite emergent initial P waves at distances of 1200 km (Fig.7g) and 1500-1600 km for the Quartz profiles (Fig.7f,h). These models also show larger secondary arrivals following immediately the initial P wave throughout the shown distance range. However, the most striking feature of these seismograms is the strong amplitude arrival following the 400 km reflection with delays between about 15 to 25 sec depending on the model and a phase velocity close to the initial P wave. This phase was found before by Ryberg (1993) in the seismic observations along the Quartz profile as an apparently longer period arrival and interpreted as the surface reflection PP. A closer investigation determines the earlier phase seen in Figs,7f-h to be the PP phase while the strong arrival can be identified as overcritical PP reflection from strong velocity gradients near 120 and 140 km depth. Therefore this phase is quite late in the Quartz models, but it is interesting to note that it appears much earlier in the model by Priestley & Cipar (1994) and might interfere and thus be interpreted as the 400 km reflection at distances less than 1600 km. If on the other

hand this arrival is close to the reflection as might be evidence in the ARU data, then the velocity models derived by Mechie et al. (1993) are either too slow in the uppermost mantle or the velocity gradient is introduced too deep. Mechie et al. (1993) argued for an alternate model for their profile line with the shot point in the north with velocities near 8.2 km/sec at those depths which in turn is close to the values found by Priestley & Cipar (1994).

From the preceding discussion of previous models it becomes evident that most of those models are inadequate in reproducing the characteristics at ARU, which, as detailed in the previous section, are an emergent P wave arrival followed by fairly high frequency secondary arrivals, which in turn are preceding a low-frequency 400 km reflection and a high frequency arrival with the dominant amplitudes within the P wave portion of the seismogram. In order to resolve the discrepancies between P observations and synthetic P wave seismograms we developed a new model that is fairly similar to the Quartz models and the model by Priestley & Cipar (1994), as these models both feature somewhat low-amplitude direct P waves and high-amplitude PP waves. The model has a fairly small positive gradient below the Moho starting with velocities of 8.2 km/sec with a rapid increase of velocities between about 110-130 km. Below an about 10 km thick lid-like structure (similar to Priestley & Cipar, 1994) we introduced a weak low-velocity zone to about 250-300 km and a 400 km discontinuity with a velocity jump from 8.64 to 9.25 km/sec. Similar values for the velocity contrast across this discontinuity were proposed for other models. The synthetic P wave seismograms for this model with frequency and slowness parameters as used in all the previous calculations are shown in Fig.8a for the vertical component and in Fig.8b for the radial component. The seismograms indicate a emergent P arrival beyond 1200-1300 km and a strong secondary arrival seen for distances less than 1800 km. The third arrival seen particularly for the distance of 1600 and 1700 km can be attributed to multiple between the Moho and the strong velocity gradient near 120 km depth. The reflection from the 400 km discontinuity appears for distances larger than 1500 km where it interferes with the surface reflection PP from both the direct wave and the 120 km gradient reflection. The radial component seismograms are somewhat at odds with the observations, as they show a similar pattern as the vertical component, however the observations do not show pronounced secondary arrivals (Fig.2b).

So far a source time function of 1 sec was used throughout all synthetic calculations. Goldstein et al. (1992) argued for a source function of 0.5 sec duration based on the

waveform matching of synthetic reflectivity seismograms and observations at NORESS which is beyond the distance where upper mantle discontinuities cause waveform complexities. In Figs.9 we used the same velocity model as in Figs.8 but applied this shorter source time function. The result from the higher frequency content of the source wavelet is an increase in amplitude for the two underside reflections (Moho/surface) related to the velocity gradient near 120 km depth, represented by the third P arrival and the arrival following the 400 km reflection, respectively at 1600 km distance. Comparing these adjacent arrivals, then it is evident that they are now about the same amplitude, while in Fig.8 the earlier arrival was higher amplitude. This behavior is somewhat consistent with the observations at ARU (e.g. Fig.3). In addition, the radial components show less significant secondary arrivals in better agreement with the ARU data.

#### **b) Complete seismograms**

Starting from the P wave models we computed complete synthetic seismograms with constrained S wave models using a Poisson's ratio of 0.25. The frequency band considered was 0.02-2Hz with a sampling interval of 0.125 sec and a phase velocity window between 3 km/sec and 16 km/sec was applied. The resulting records are shown in Fig.10a-b for the representative models CE200 (Goldstein et al., 1992) and Quartz-N (Mechie et al., 1993) for comparison with the most important features in the observed S waveforms and a qualitative discussion in this section. Although CE200 was found to exhibit major deficiencies in explaining the P wave portion, it was shown by Goldstein et al. (1992) that the surface wave dispersion in the frequency band from 10-100 sec is quite well matched. The complete seismograms show an impulsive Lg arriving 250 sec into the reduced time trace at 1500 km which is slightly earlier than indicated by the S wave observations (see Fig.2) and surface waves that are predicted to arrive after 300 sec. The crustal velocities ranging from 3.6 to 3.9 km/sec as used by the constrained S wave model are therefore slightly higher than observed which is consistent with Goldstein's dispersion curves where the observed dispersion is consistently slower than the prediction. The initial S wave with onset about 150 sec after the initial P wave at 1500 km from their model is much earlier than the observed first S wave arrival at ARU at a slightly larger distance. Interesting from these model seismograms is also the significant amplitude for the S wave reflection from the 400 km discontinuity for distances beyond 1600 km. Unfortunately, this arrival is not well developed for distances

similar to GAR and ARU and therefore can not be used for estimation of the S wave velocity contrast across this discontinuity.

The synthetic seismograms from the constrained Quartz-N model by Mechie et al. (1993) are shown in Fig.10b and show some interesting similarities with the observations. Although the Lg wave is quite emergent due to the lack of a gradient within the crust, the steady increase of S wave amplitudes between the initial S (150 sec after P at 1500 km) and the Lg/surface wave arrival matches the pattern observed at ARU. This model with a small velocity contrast across the 400 km discontinuity does not produce a strong reflection within the considered distance range.

To summarize the results from the complete seismogram calculation we find that the crustal model used by Goldstein et al, (1992) gives a good match of surface waves and Lg observations with the deficiency of velocities slightly too high. Considerable positive velocity gradients as present for the Quartz-N model within depths of 100 km below the Moho produces increasing amplitudes following the initial S wave arrival. Models with positive gradient below the Moho such as KCA (King & Calcagnile, 1976) or K8 (Given & Helmberger, 1980) produce similar results. A suitable S wave model for the ARU observations must include the aforementioned features, however all constrained models predict considerably earlier mantle S arrivals. Therefore the Poisson's ratio below the Moho in Central Asia must be higher than 0.25.

### Discussion and Conclusions

Far-regional observations at ARU have been used to constrain upper mantle velocity structure in Central Eurasia by testing previously published P wave models. Synthetic seismograms based on the extended reflectivity suggest several later phases in the early P wave segment that were previously interpreted as reflections from velocity discontinuities near 200 and 400 km by Goldstein et al. (1992), but that can be identified as surface and Moho underside reflections. The model calculations also were successful in predicting the higher frequency contents of the surface reflection relative to the 400 km reflection and shows that these two phases interfere at ranges close to the distance between ARU and the East Kazakhstan test site. The slowness estimates made by Goldstein et al. (1992) for their second arrival supports these findings as they find higher slowness than for the initial P arrival in

agreement with slower phase velocities for secondary arrivals found in this study. Measured slowness for arrivals 3 and 4 in Goldstein et al. (1992) can also be explained by the synthetic seismograms shown in Figs 8 and 9, in that the surface reflection PP interfering with the 400 km reflection at ARU producing the broad slowness estimate for arrival 3. The estimate for arrival 4 is dominated by the coherent long-period 400 km discontinuity reflection, the following high-frequency, high-amplitude arrival does not contribute significantly, possibly due to incoherence.

The significance of surface reflections in far-regional observations was furthermore stressed by Ryberg (1993) which follows the initial P arrival by about 10 sec. The secondary arrival in Figs 8 and 9 which is a overcritical arrival produced by the strong gradient near 120 km is seen in many DSS profiles between 800 and at least 1500 km, as argued by Mechie et al. (1993) or Ryberg (1993). Ryberg(1993) modeled this arrival with a laminated zone right below the Moho and produced an arrival that was significant in amplitudes to at least 3000 km. The much simpler model used here supports the fact that secondary energy following the initial P arrival at far-regional distances in Central Eurasia results from mantle P waves that propagate in a about 80-100 km thick zone below the Moho.

The preliminary study of complete seismograms argues for stronger positive gradients of the shear velocity structure of at least the top 100 km in the shear velocity structure in the upper mantle. The models used throughout this study predict initial S arrivals much earlier than observed by as much as 20 sec which in turn would predict Poisson's ratios larger than 0.25 for the upper mantle in Central Eurasia. More modeling is required in order to resolve these discrepancies. The modeling also produced strong S reflections for models with significant 400 km discontinuities, however, these arrivals become only large for distances well beyond the distance between ARU and the East Kazakhstan test site. Future analysis of the S waves from deep seismic sounding profiles could focus on identifying this phase and its implication for the shear velocity structure near the discontinuity.

### Acknowledgments

This research was supported by the Air Force Phillips Laboratory under contract F19628-91-K-0016.

## References

- Benz, H.M. Unger, J.D. Leith, W.S., Mooney, W.D., Solodilov, L., Egorkin, A.V. & Ryaboy, V.Z. (1992): Deep seismic sounding in northern Eurasia, EOS, 73, 297-300
- Brüstle, W. & G.Müller (1983): Moment and duration of shallow earthquakes from Love-wave modeling for regional distances, Phys.Earth Planet.Int., 32, 312-324
- Der, Z., Lees,A. & Cormier, V. (1986): Frequency dependence of Q in the mantle underlying the shield areas of Eurasia, Part III: The Q model, Geophys. J.R. astr. Soc., 87,1103,1112
- Dziewonski,A.M, S.Bloch & M.Landisman (1969): A technique for the analysis of transient seismic signals, Bull.Seism.Soc.Am., 59, 429-444
- Given, J.W. & D.V. Helmberger (1980): Upper mantle structure beneath north-western Eurasia, J.Geophys.Res., 85, 7183-7194
- Goldstein,P., Walter, W.R. & Zandt, G. (1992): Upper mantle structure beneath central Eurasia using a source array of nuclear explosions and waveforms at regional distances, J.Geophys.Res., 97, 14097-14113
- King, D.W. & Calcagnile,G. (1976): P wave velocities in the upper mantle beneath Fennoscandia and western Russia, Geophys. J.R. astr. Soc., 46, 407-432
- Koch, K. & B.Stump (1993): Implications for upper mantle structure in the Western United States from complete far-regional seismograms, submitted to Bull.Seism.Soc.Am.
- Lefevre, L.V. & Helmberger, D.V. (1989): Upper mantle P-wave velocity structure of the Canadian shield, J.Geophys.Res., 94, 17749-17766
- Mechie, J., Egorkin, A.V., Fuchs, K., Ryberg, T., Solodilov, L. & Wenzel,F. (1993): P wave mantle velocity structure beneath northern Eurasia from long-range recordings along the profile Quartz, Phys. Earth Planet. Int, 79, 269-286
- Müller, G. (1985): The reflectivity method: a tutorial, J. Geophys., 58, 153-174
- Pavlenkova, N.I. & Yegorkin, A.V. (1983): Upper mantle heterogeneities in the northern part of Eurasia, Phys. Earth Planet. Int, 33, 180-191
- Priestley, K. & Cipar, J. (1994): Upper mantle velocity structure beneath the Siberian platform, AFPL report PL-TR-94-2017, 46-66 , ADA276729
- Ryberg,T. (1993): Seismische Modellierung mit höheren Gaußbeammmoden und Interpretation tiefenseismischer Daten des Profiles Quartz, PhD. thesis, University Karlsruhe, 102 p.



Vinnik, L.P. & Ryaboy, V.Z. (1981): Deep structure of the East European platform according to seismic data, *Phys. Earth Planet. Int.*, 25, 27-37

Yegorkin, A.V. & Pavlenkova, N.I. (1993): Studies of mantle structure of U.S.S.R territory on long-range seismic profiles, *Phys. Earth Planet. Int.*, 25, 12-26

**Table 1: Summary of explosion parameters <sup>o)</sup>**

No.	Date	Origin Time	Latitude	Longitude	m <sub>b</sub>	Range <sup>†)</sup>
1 <sup>‡)</sup>	10/18/1988(292)	034009.2	49.802N	78.002E	4.9	1488
2 <sup>‡)</sup>	02/17/1989(048)	040109.2	49.849N	78.064E	5.0	1489
3 <sup>‡)</sup>	11/23/1988(328)	035709.0	49.765N	78.029E	5.3	1492
4	02/12/1989(043)	041509.2	49.911N	78.704E	5.9	1521
5	01/22/1989(022)	035709.0	49.945N	78.815E	6.0	1526
6	07/08/1989(189)	034700.0	49.872N	78.767E	5.6	1528
7 <sup>‡)</sup>	11/12/1988(317)	033006.3	50.050N	78.968E	5.3	1528
8	09/14/1988(258)	035959.7	49.882N	78.822E	6.1	1530
9 <sup>‡)</sup>	09/02/1989(245)	041659.8	50.017N	78.983E	5.0	1531
10	10/19/1989(292)	094959.8	49.925N	78.907E	5.9	1532
11	12/17/1988(352)	041832.2	49.883N	78.922E	5.9	1536

<sup>o)</sup> From Goldstein et al. (1992)

<sup>†)</sup> Epicentral distance (in km) to Arti (ARU)

<sup>‡)</sup> Events with low signal/noise ratio (not used throughout this study)

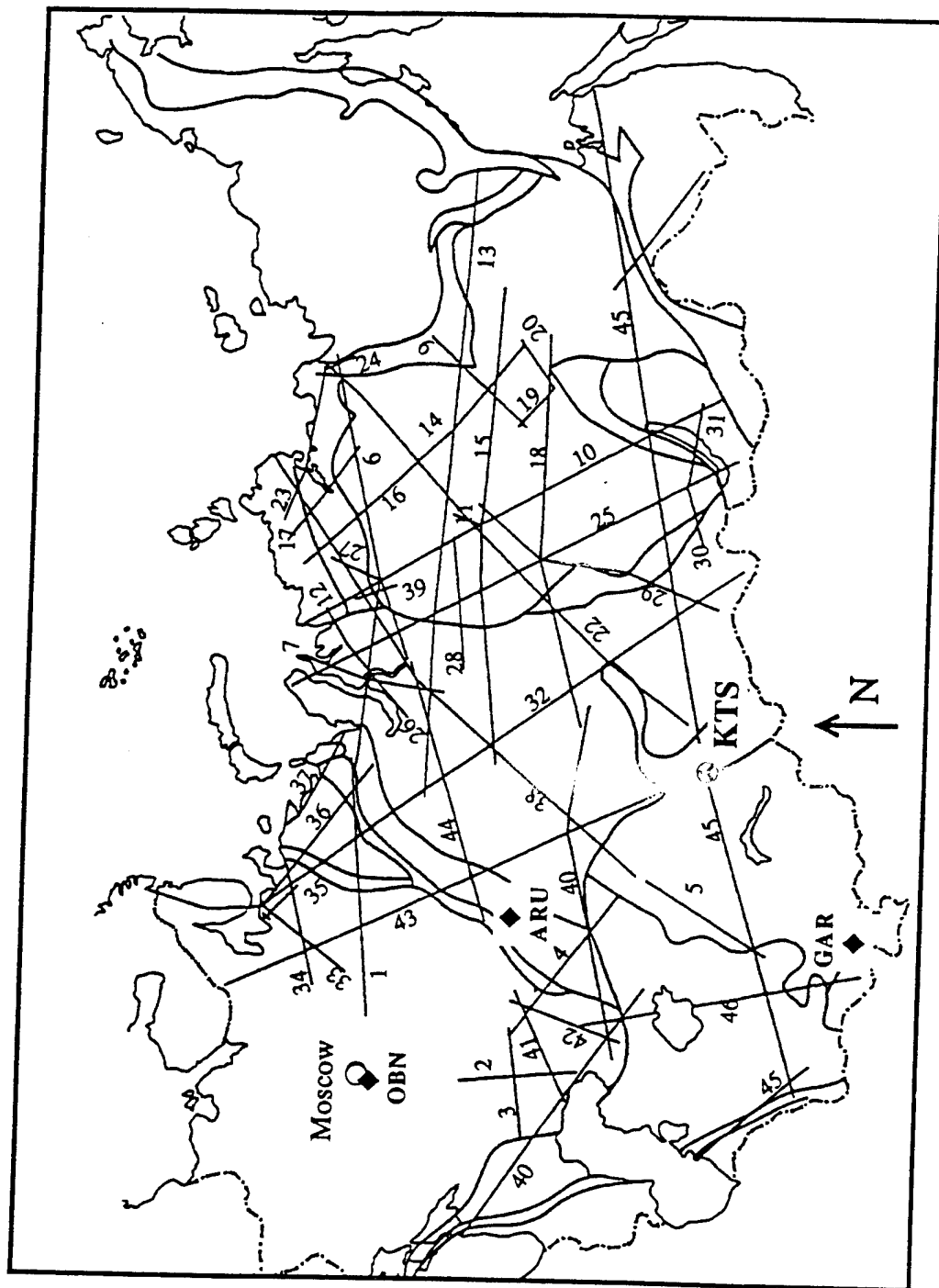


Figure 1: Map of station and event locations including deep seismic sounding profiles and main tectonic features (adapted from Ryberg (1993))

ARU – vertical component (raw data)

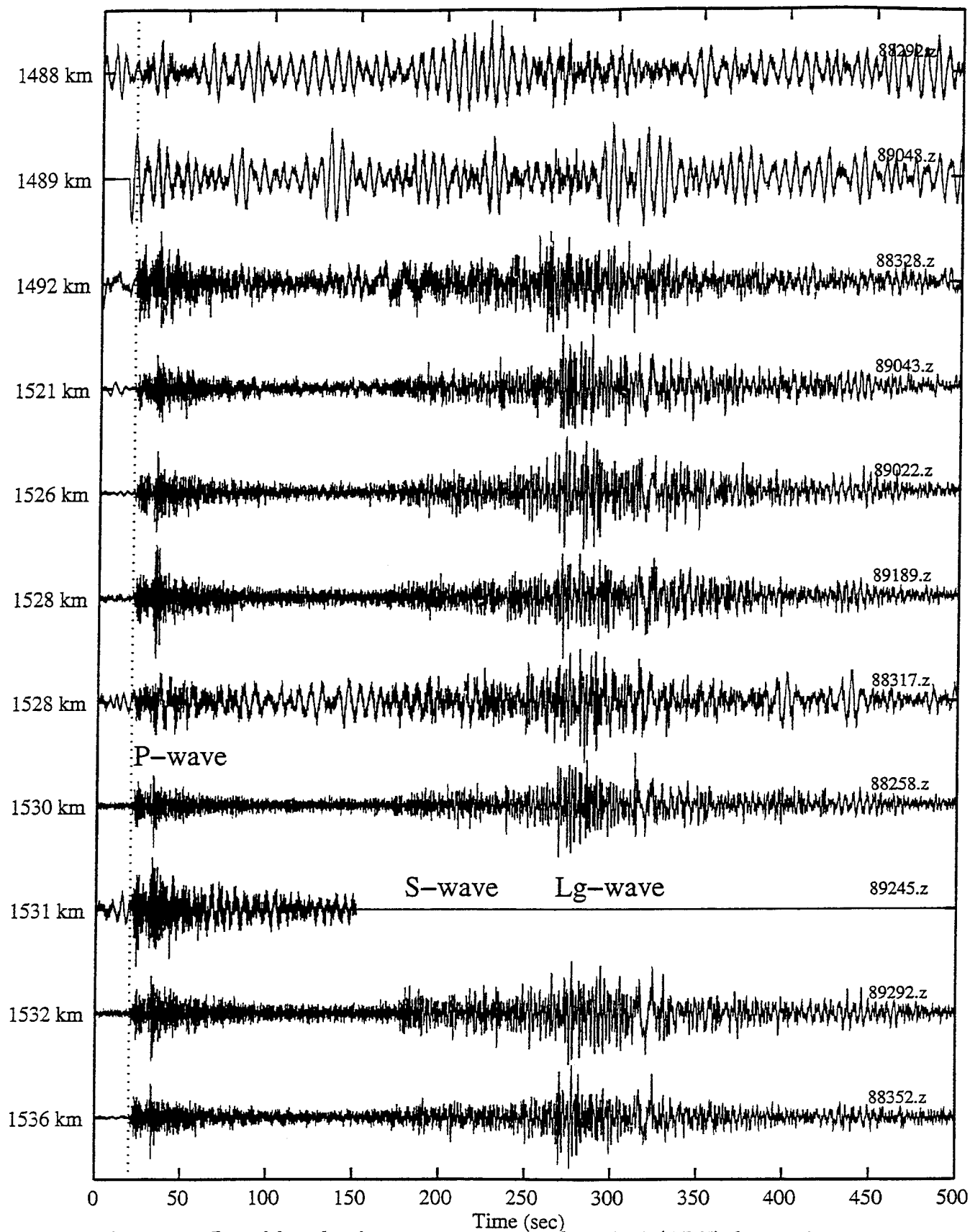


Figure 2: Broad-band seismograms observed at Arti (ARU) for explosion events studied by Goldstein et al. (1992); (a) vertical component (unfiltered) - (b) radial component (unfiltered). Epicentral distance is given to the left of trace. Only the traces 4,5,6,8,10 and 11 (from the top) are used in the following due to sufficient signal/noise ratio.

ARU - Radial component (raw data)

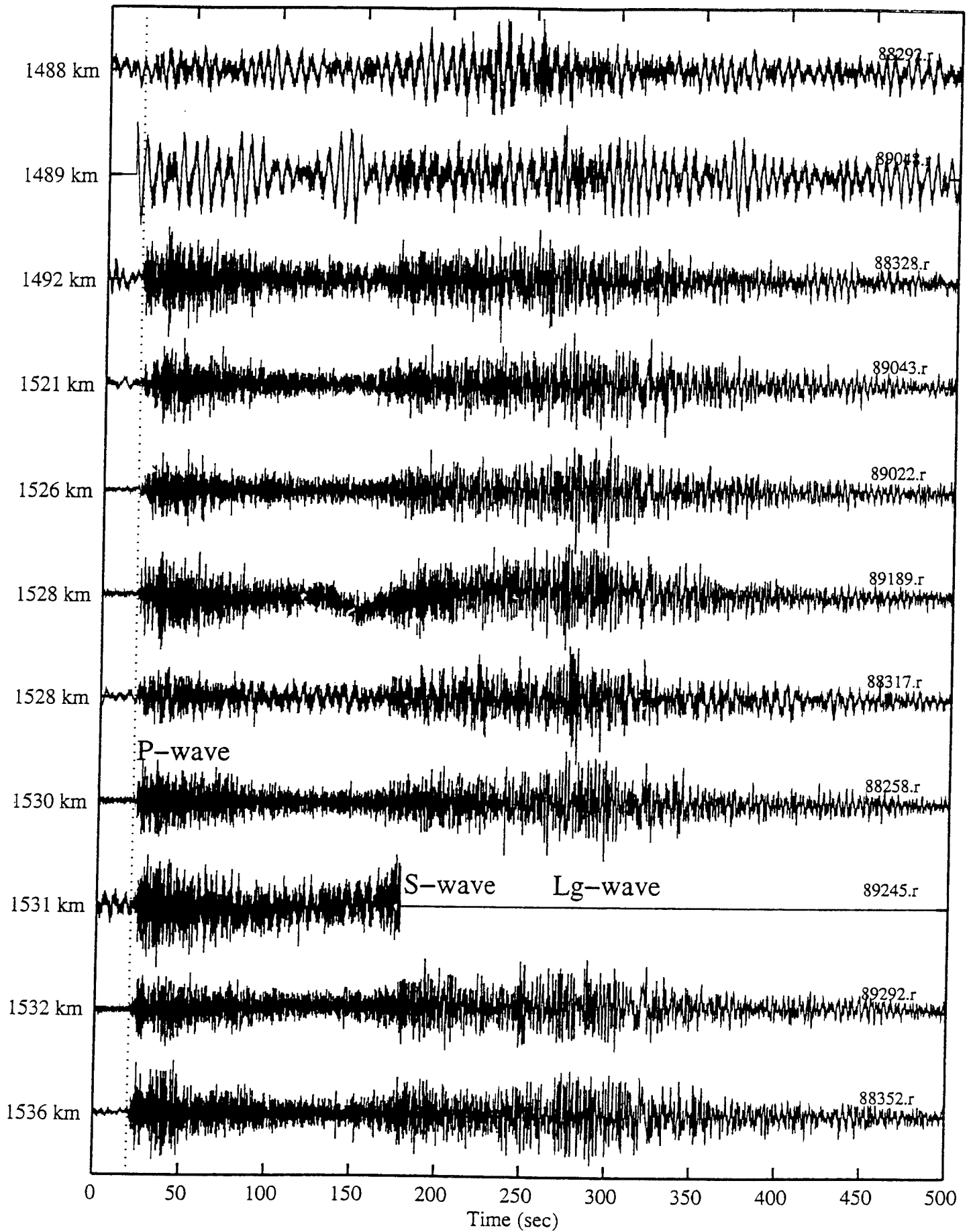
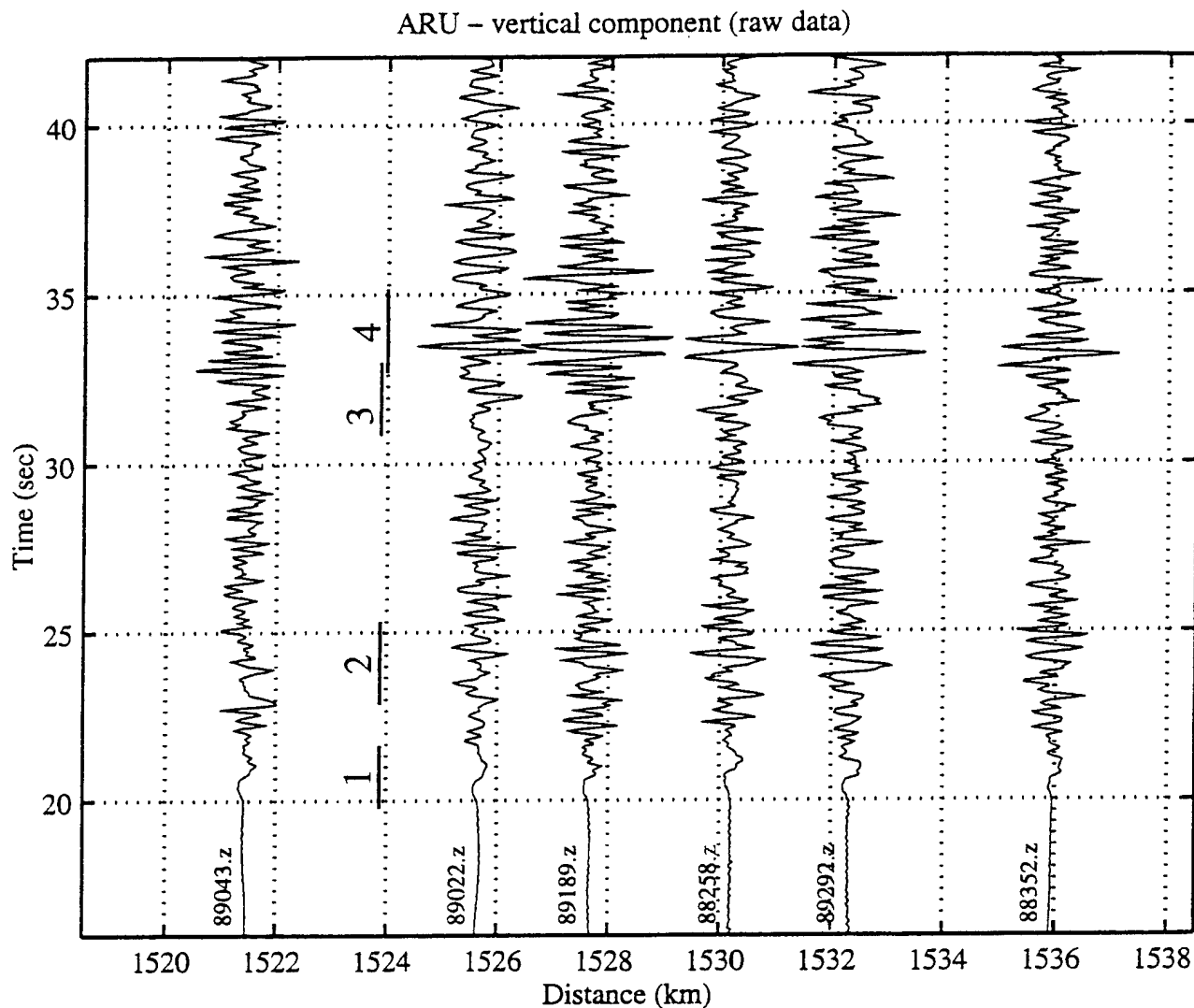


Figure 2b



**Figure 3:** P wave section of data displayed in Fig. 2a - (a) raw seismograms (b) filtered (0.2-1 Hz / 6 poles / zero-phase) - emphasizing the initial P arrival and the reflection from the 400-km discontinuity (c) P wave portion of the JVE explosion (Sept. 14, 1988) at ARU filtered in several pass-bands. When looking at longer periods, the initial P wave and the 400 km discontinuity with a stable amplitude ratio of about 1:2 remain while the second and fourth arrival disappear.

ARU - vertical component (BP 0.2-1 Hz [-2])

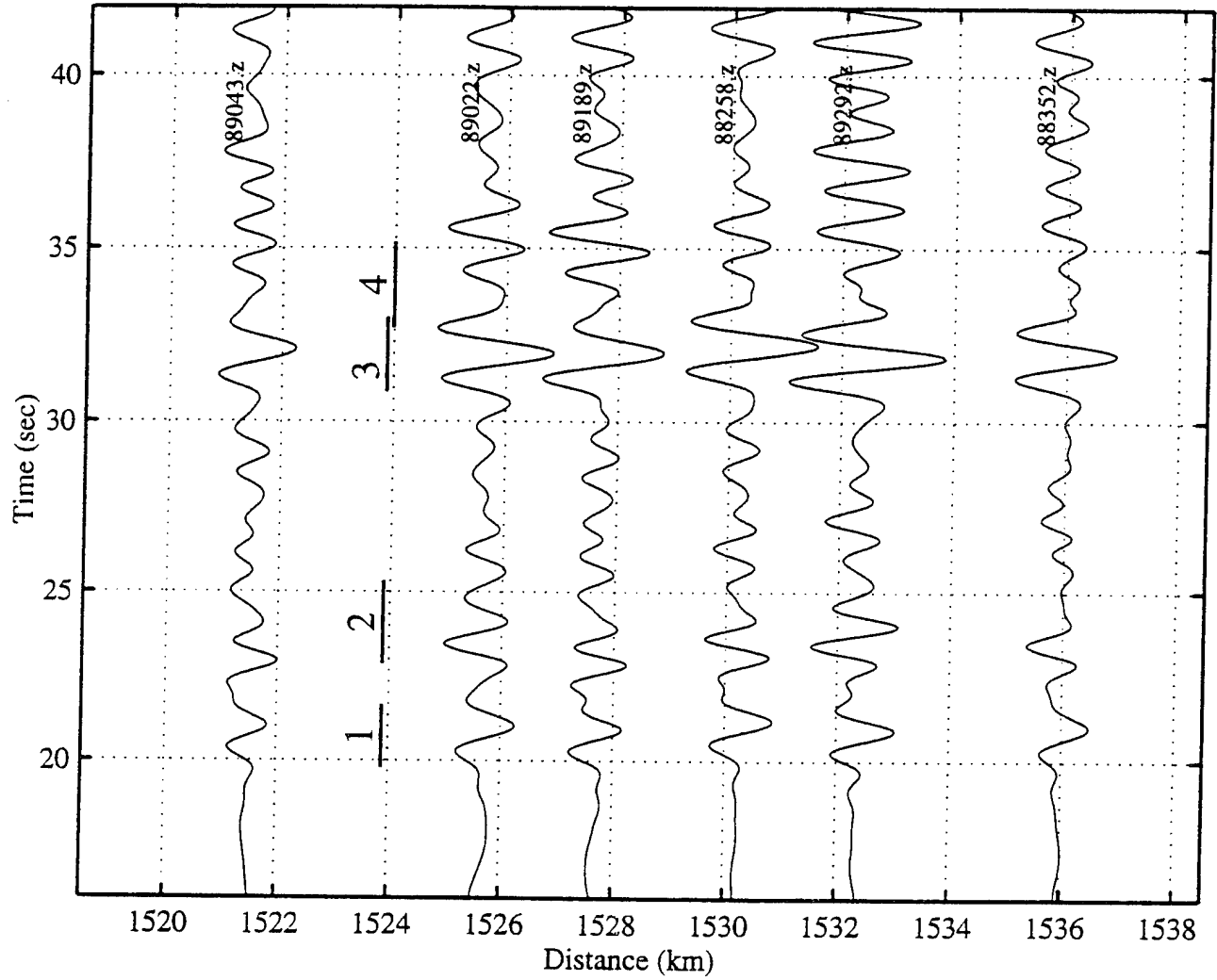


Figure 3b

ARU - vertical component (zero phase band-passed filtered)

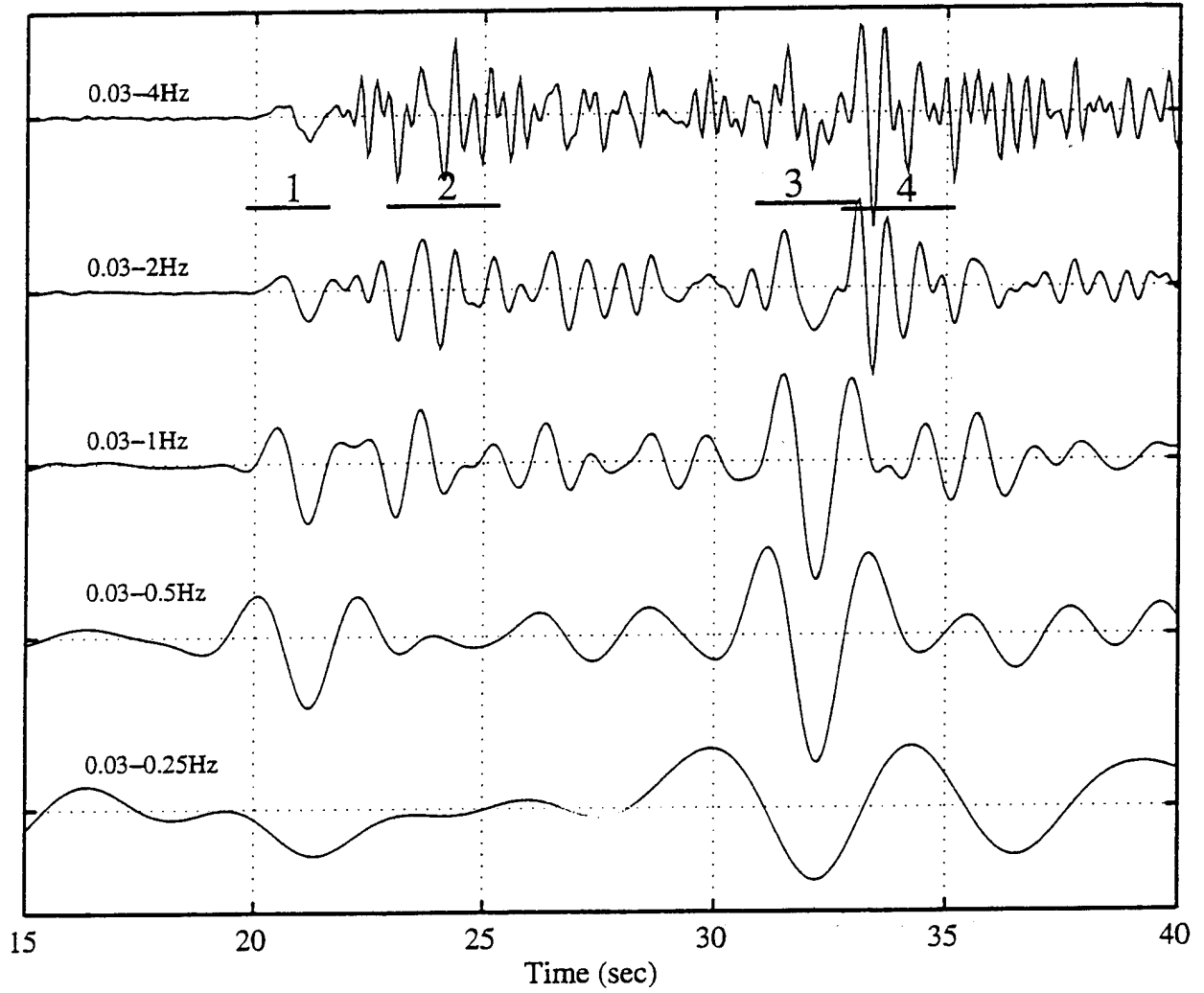
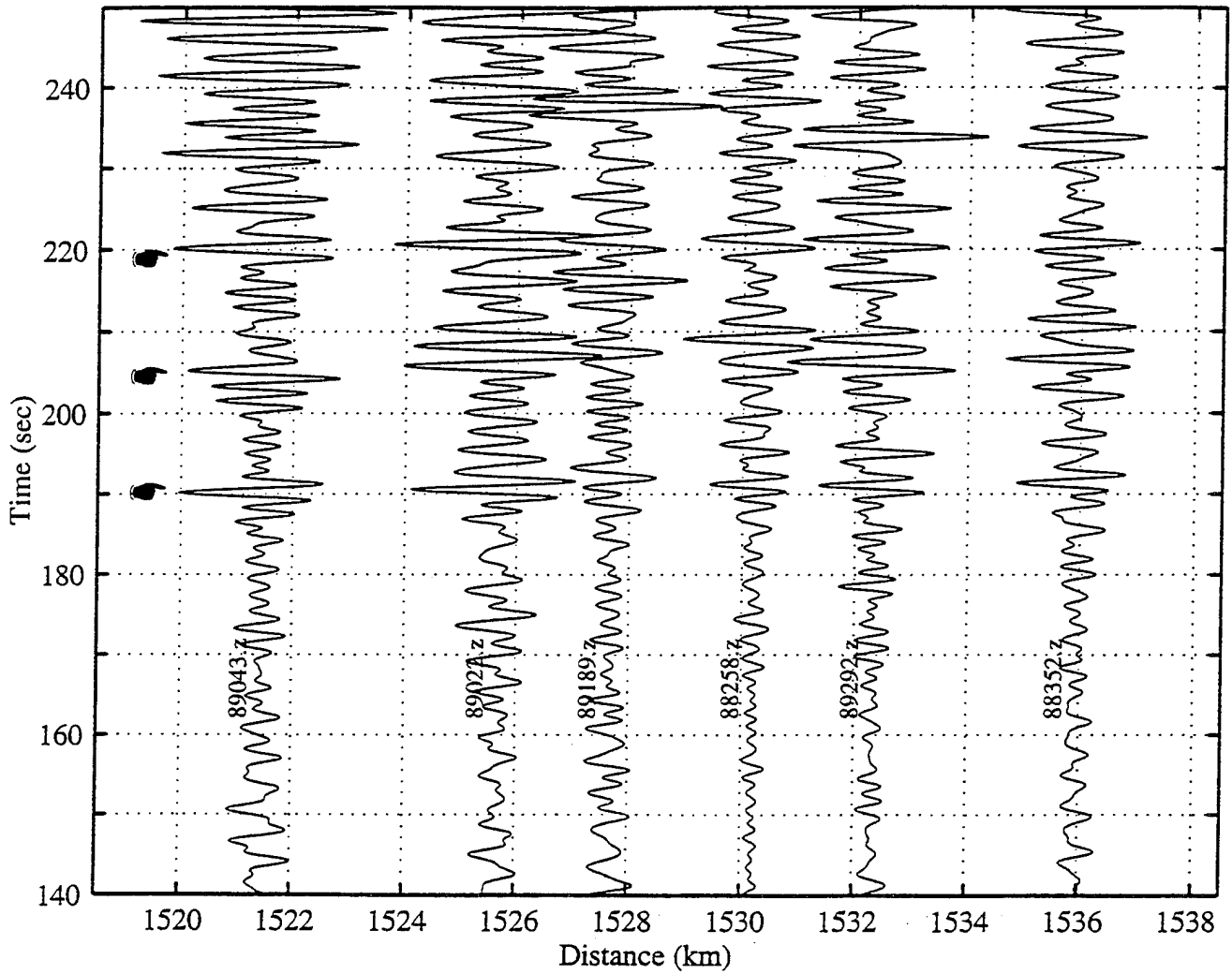


Figure 3c



ARU - vertical component (BP 0.2-0.6 Hz [-2])



**Figure 4.** (a) S wave seismogram section band-pass filtered from 0.2-0.6 Hz showing mantle S wave arrivals at 170, 208 and 220 sec after the initial P which are related to the direct S (from the near-source surface conversion) the 400 km reflection and SS - (b) Surface wave section for the 10-50 sec pass band; most of the energy is from the Airy phase with periods closed to 20 sec with group velocities of about 3 km/sec.

ARU - vertical component (BP 10-50 sec [-2])

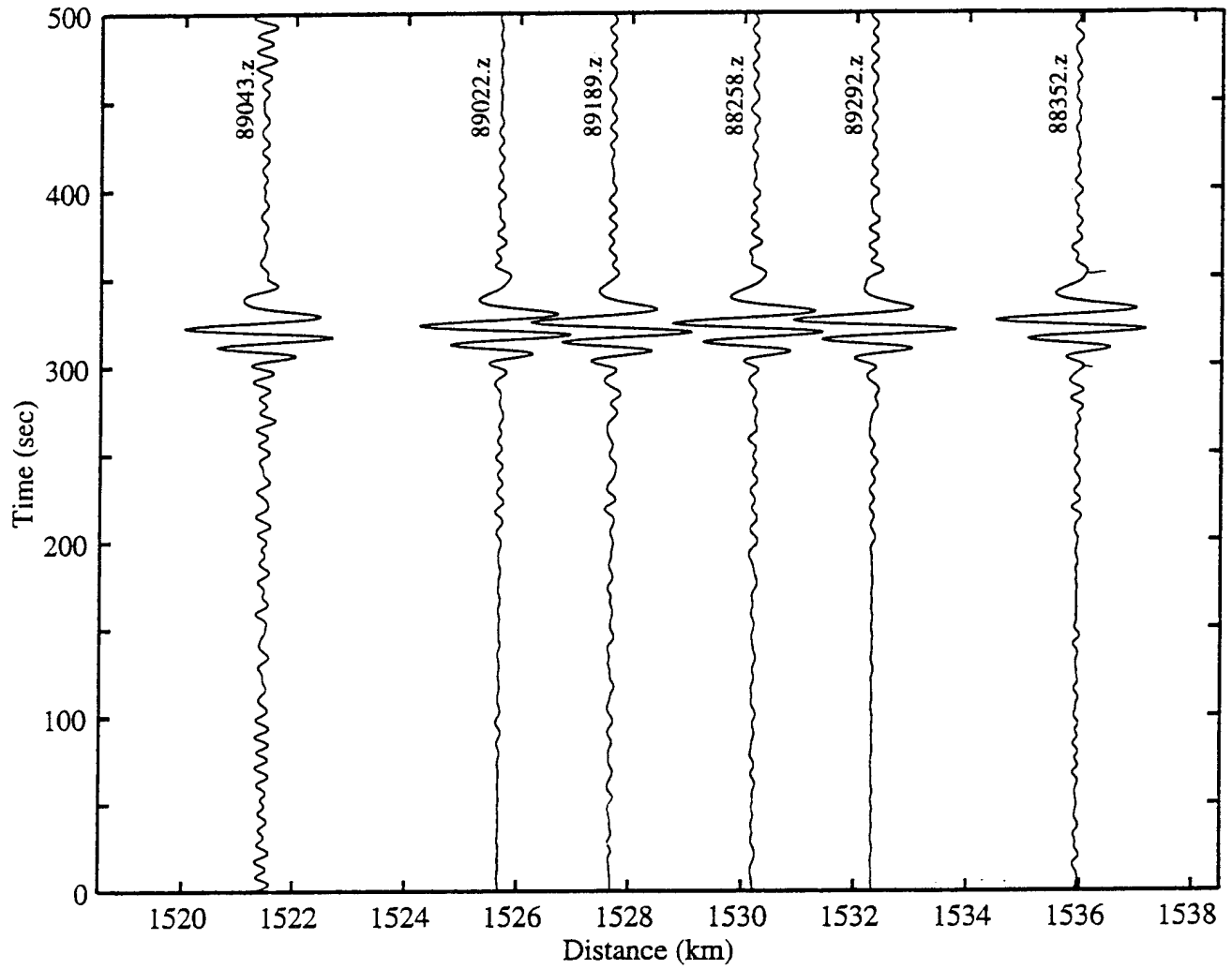
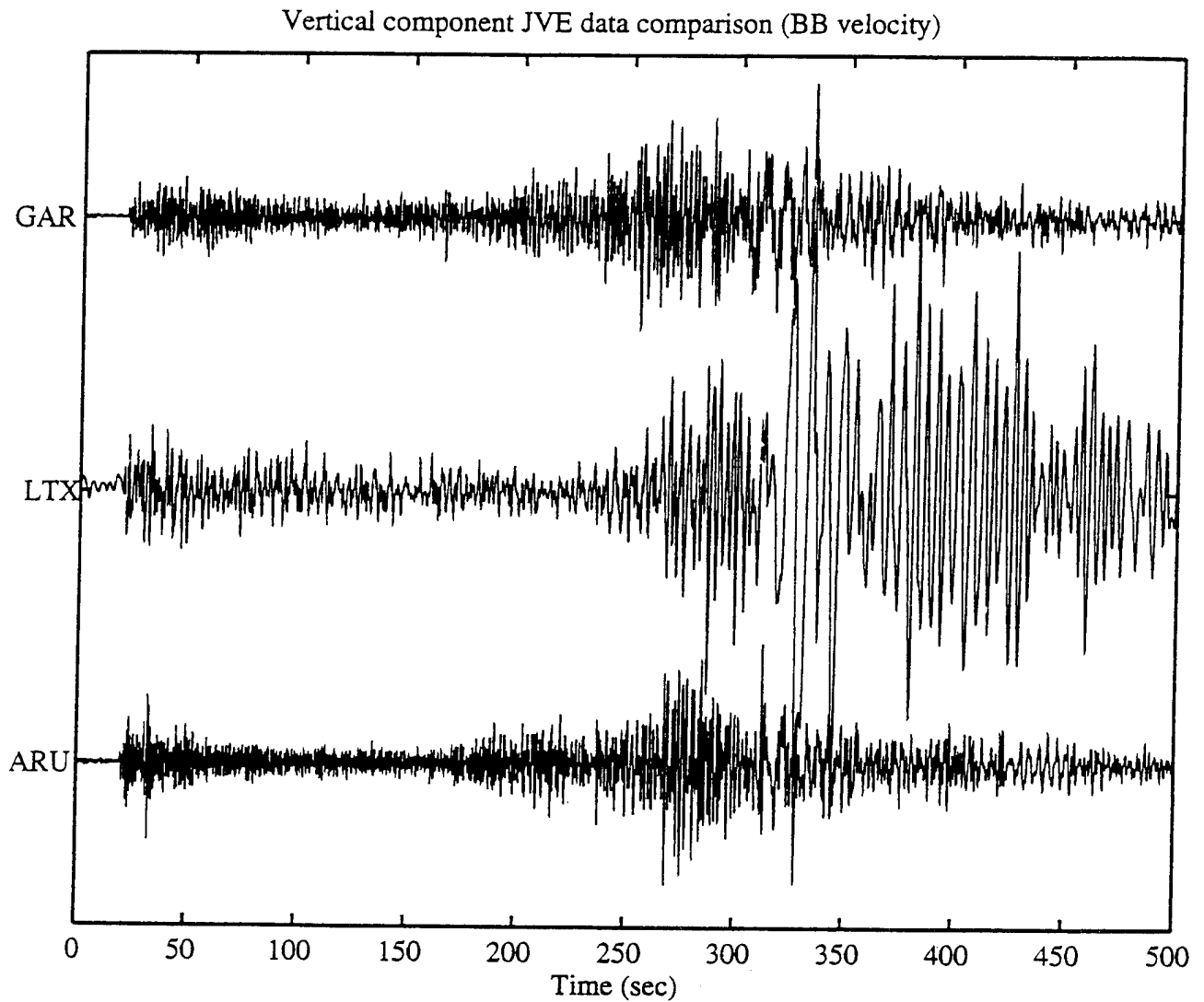


Figure 4b



**Figure 5:** Comparison of the JVE explosion waveforms at regional distances in Central Eurasia recorded at GAR (1384 km) and ARU (1530 km) (Sep. 14, 1988), and Western United States recorded at LTX (1468 km) (Aug. 17, 1988); (a) raw data featuring mantle P, Lg and mantle S only for Eurasian paths - (b) band-pass filtered P waveforms with direct P and 400 km reflection - (c) LTX P wave segment filtered in in the pass-bands given next to trace

Vertical component JVE data (BB vel.) comparison (BP 0.1-0.5Hz [-2])

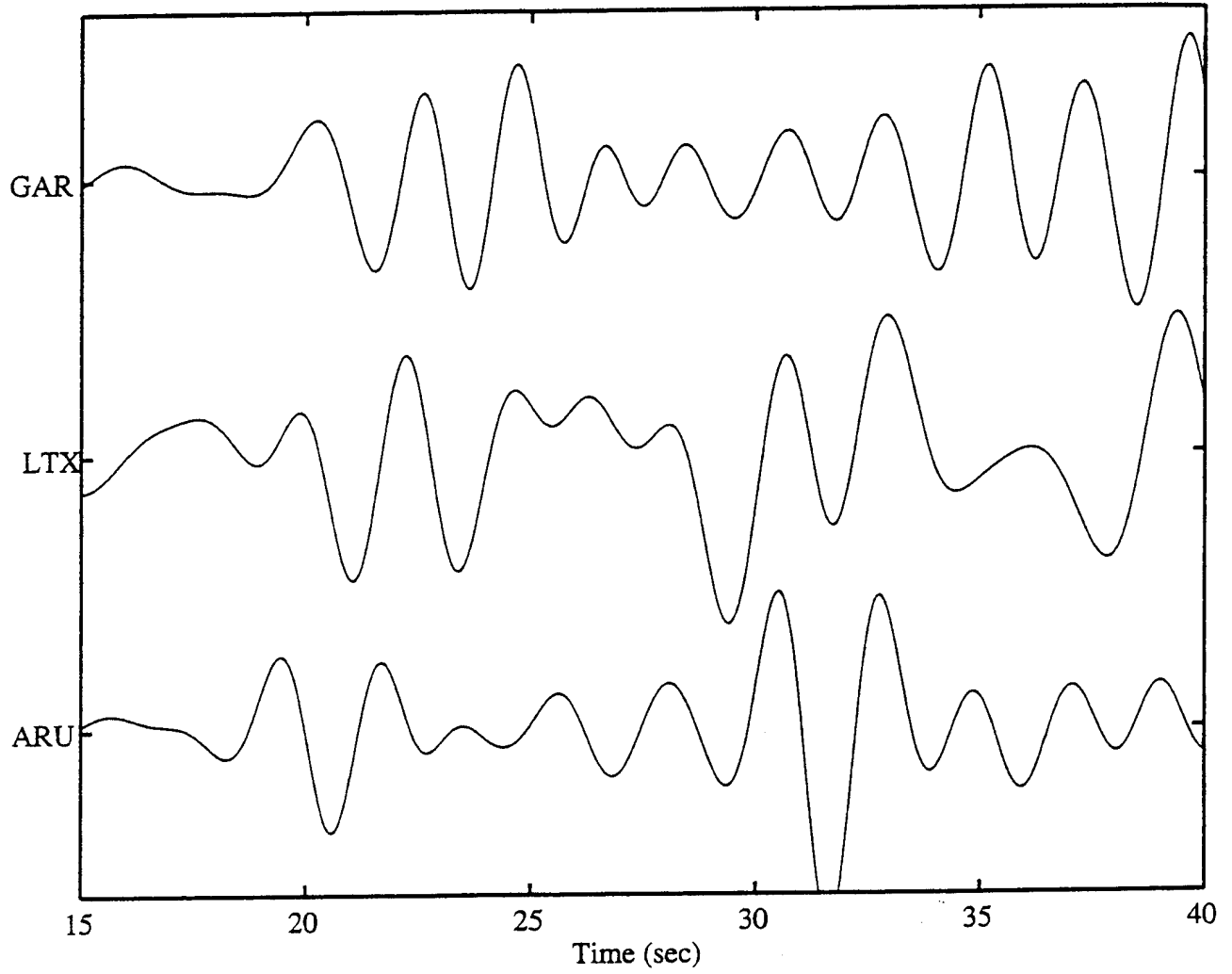


Figure 5b

Event 88\_230 at 1468.2 km (BB-integr.)

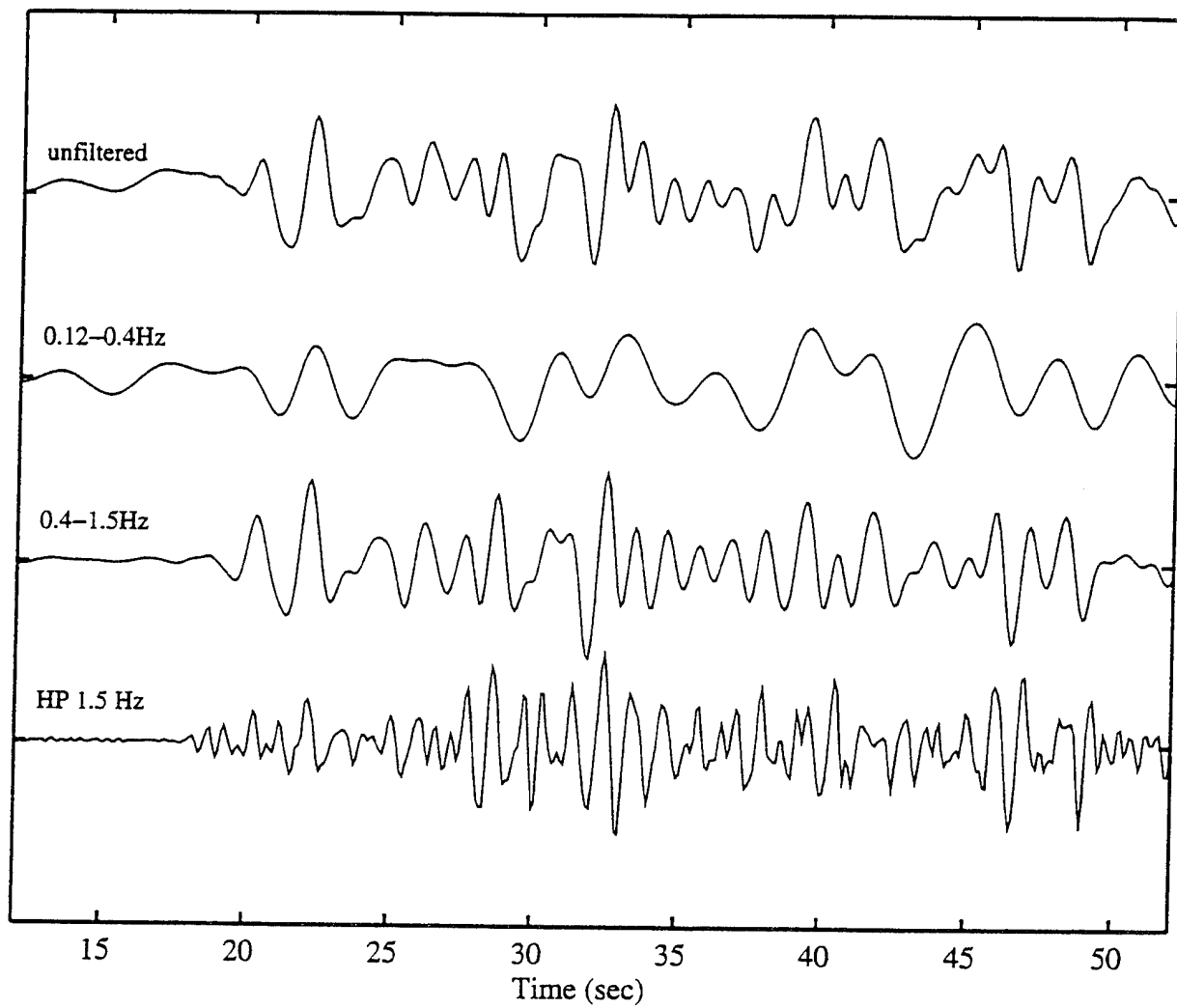
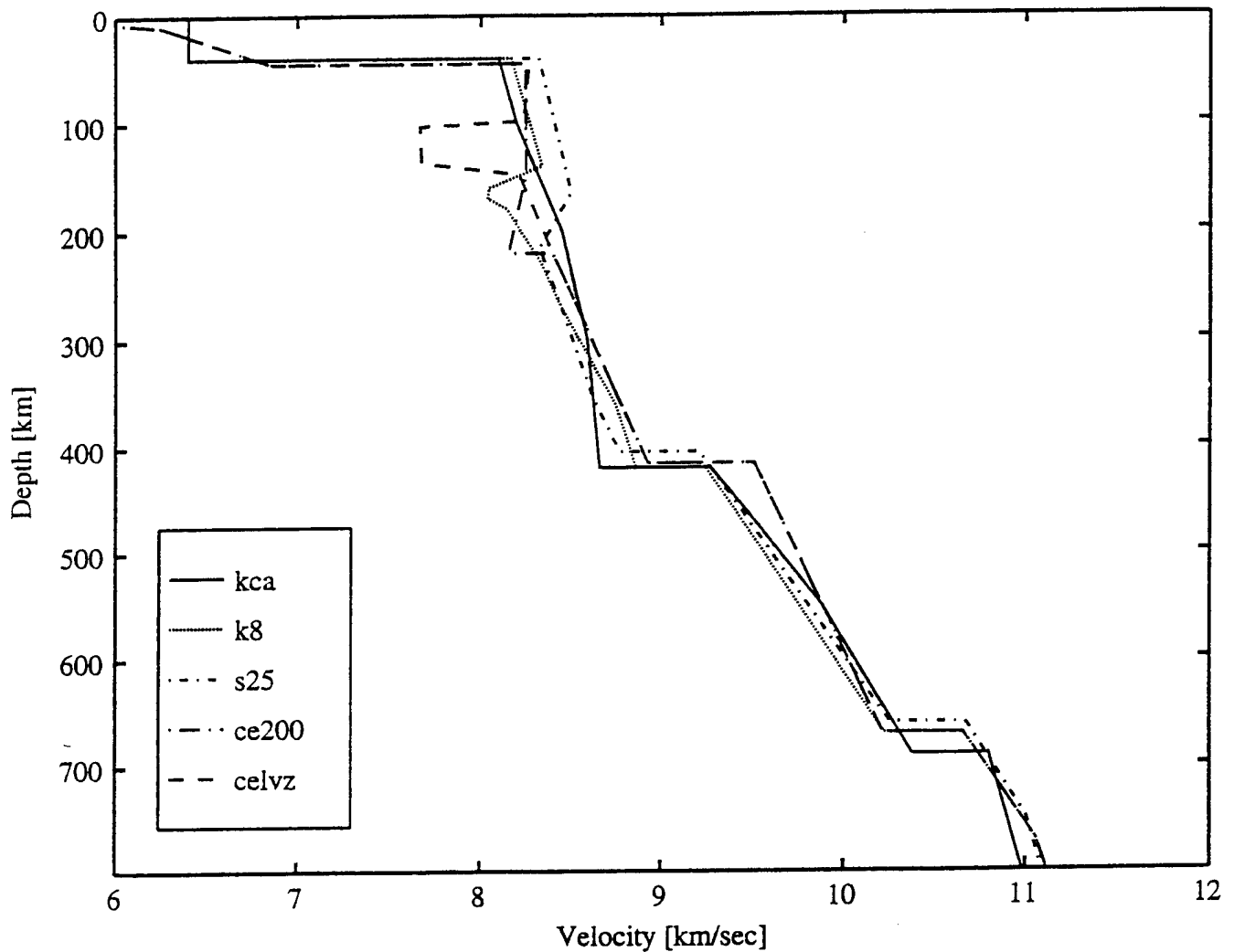


Figure 5c



**Figure 6:** Upper mantle models for stable continental regions (Eurasia):  
 (a) KCA [King & Calcagnile (1976)], K8 [Helmberger & Given (1980)], CE200/CELVZ [Goldstein et al. (1992)], S25 [Lefevre & Helmberger (1989)]  
 (b) Quartz-N/S [Mechie et al. (1993)], PRCIP [Priestley & Cipar (1994)], VKRY [Vinnik & Ryaboy (1981)], This Study

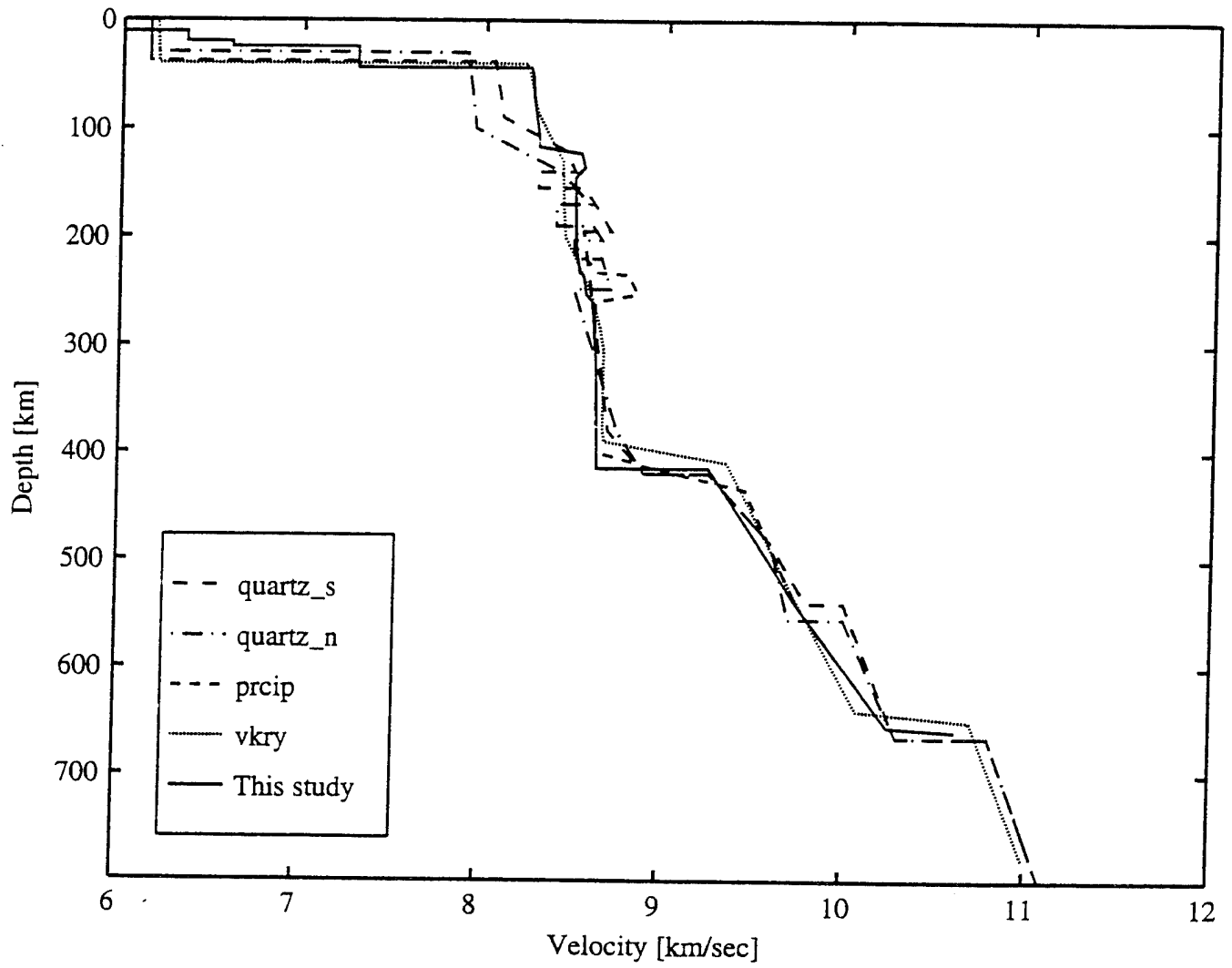


Figure 6b

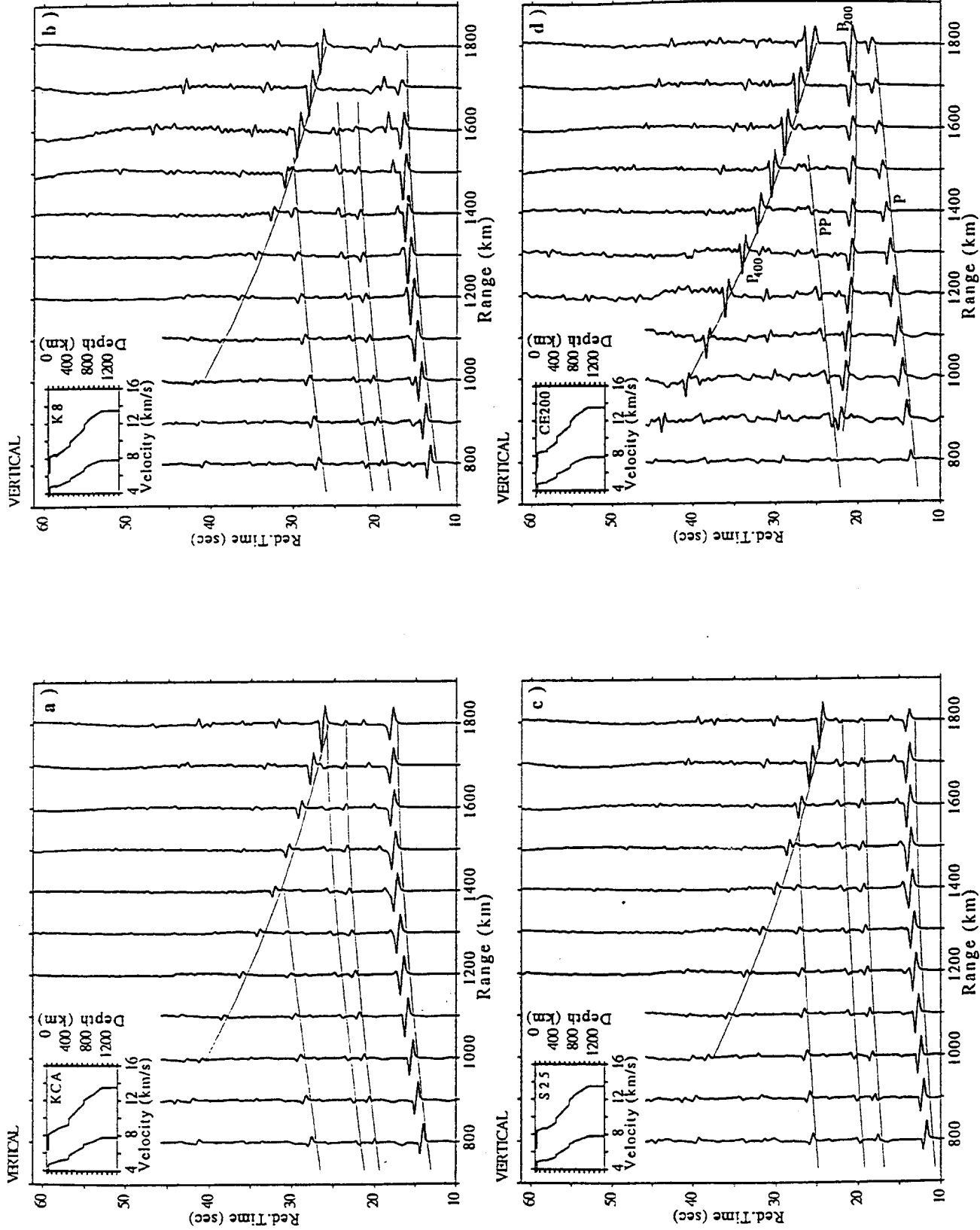


Figure 7: Synthetic P wave seismograms for various models: (a) KCA [King & Calcagnile (1976)] - (b) K8 [Helmberger & Given (1980)] - (c) CE200 [Goldstein et al. (1992)] - (d) S25 [Lefevre & Helmberger (1989)] - (e) VKRY [Vinnik & Ryaboy (1981)] - (f) Quartz-N [Mechie et al. (1993)] - (g) PRCIP [Priestley & Cipar (1994)] - (h) Quartz-S [Mechie et al. (1993)] - reduction velocity used was 8.7km/sec.



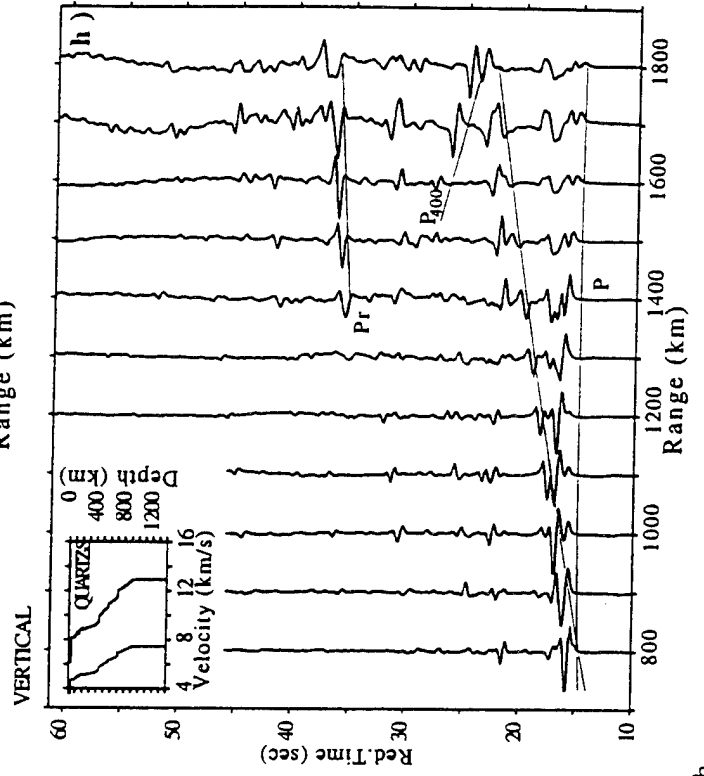
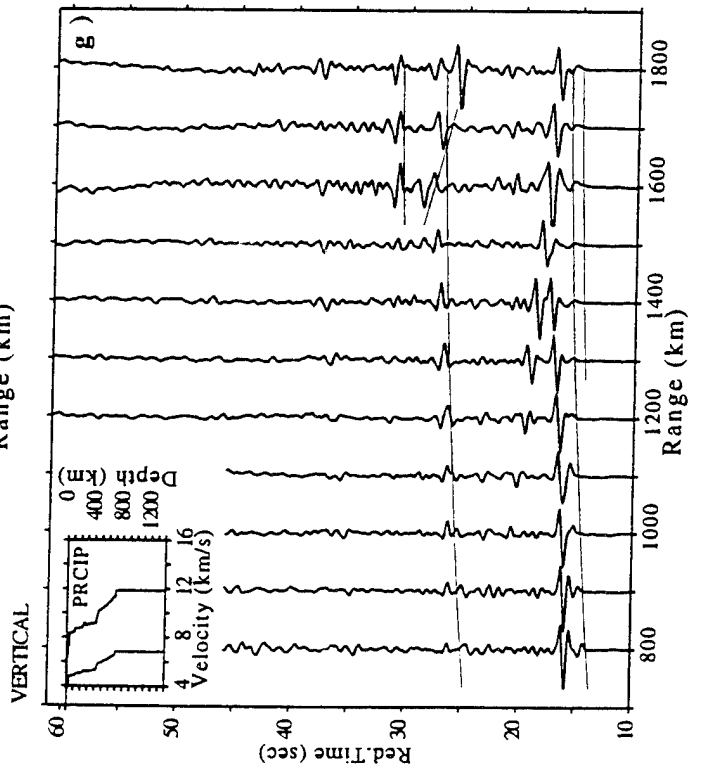
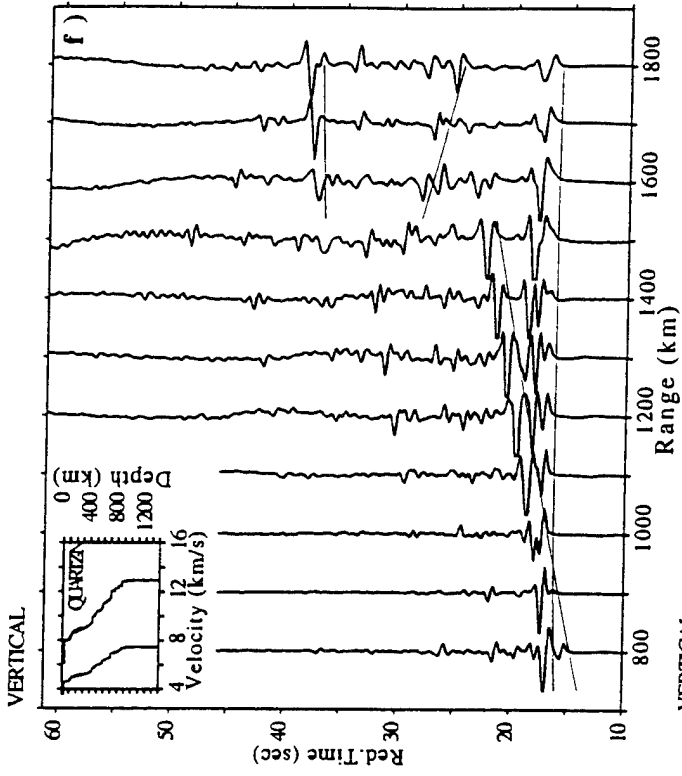
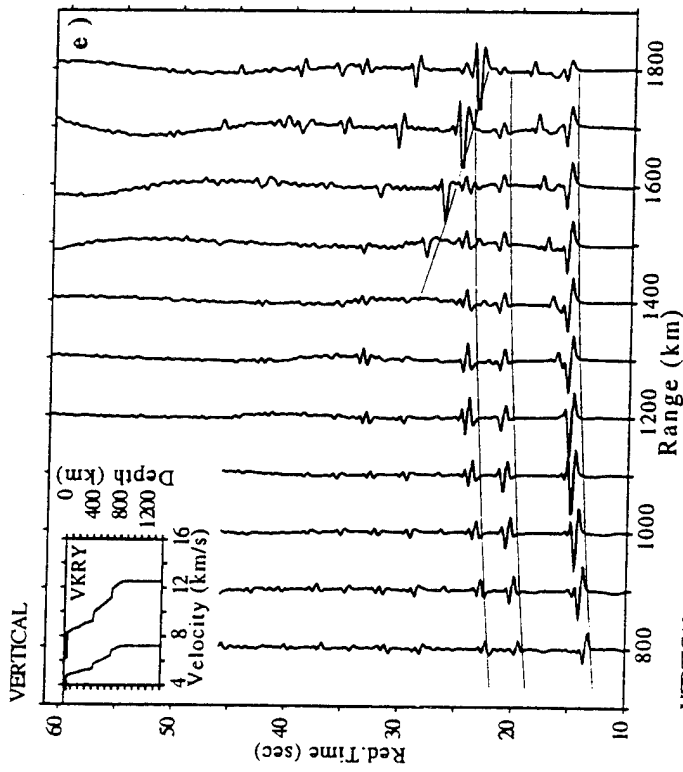


Figure 7e-h

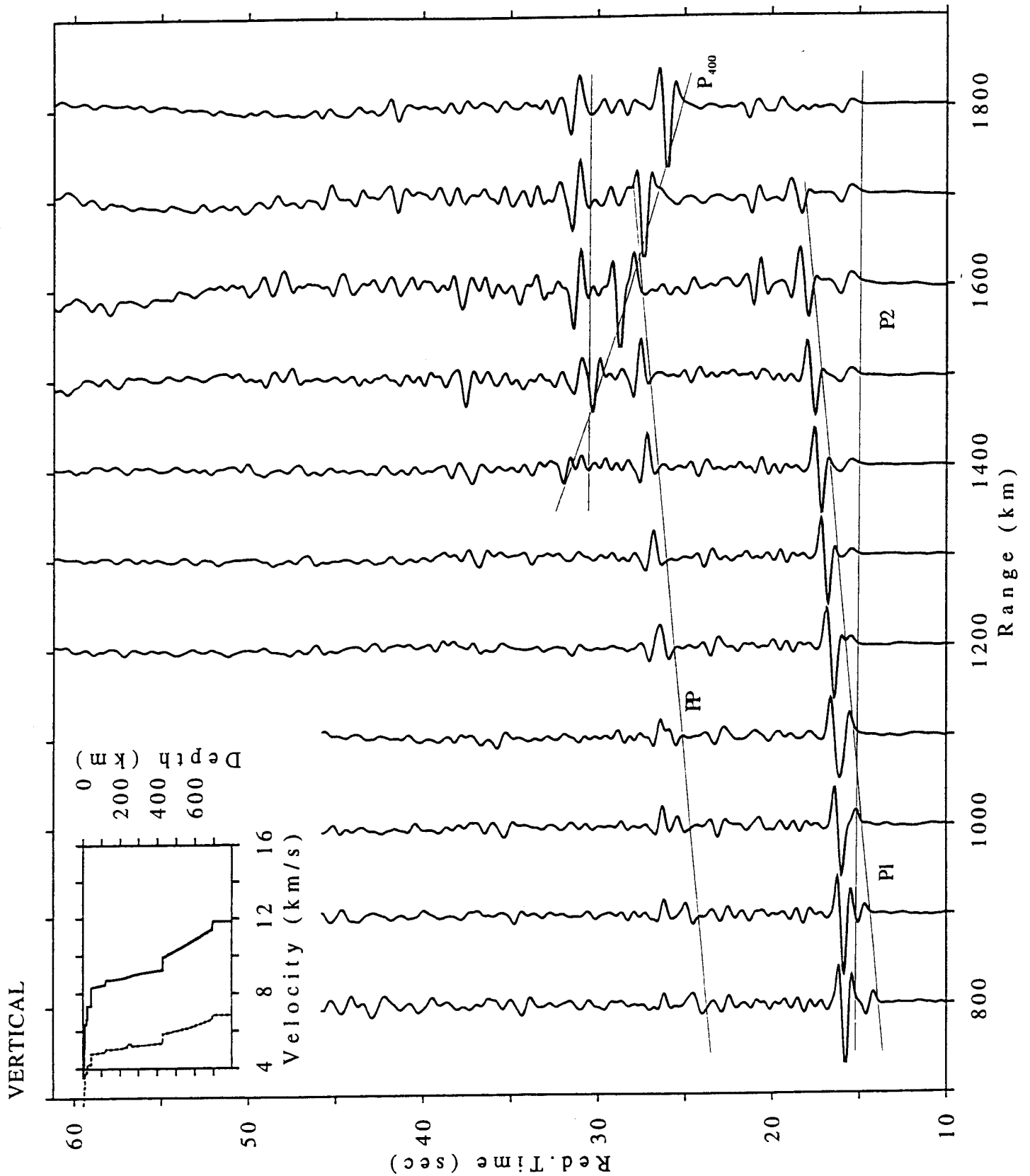


Figure 8: Synthetic seismograms for the P wave segment of the preferred model using a Bruestle-Müller source time function of 1 sec duration; (a) vertical component seismograms, (b) radial component seismograms (reduction velocity: 8.7km/sec).

HORIZONTAL

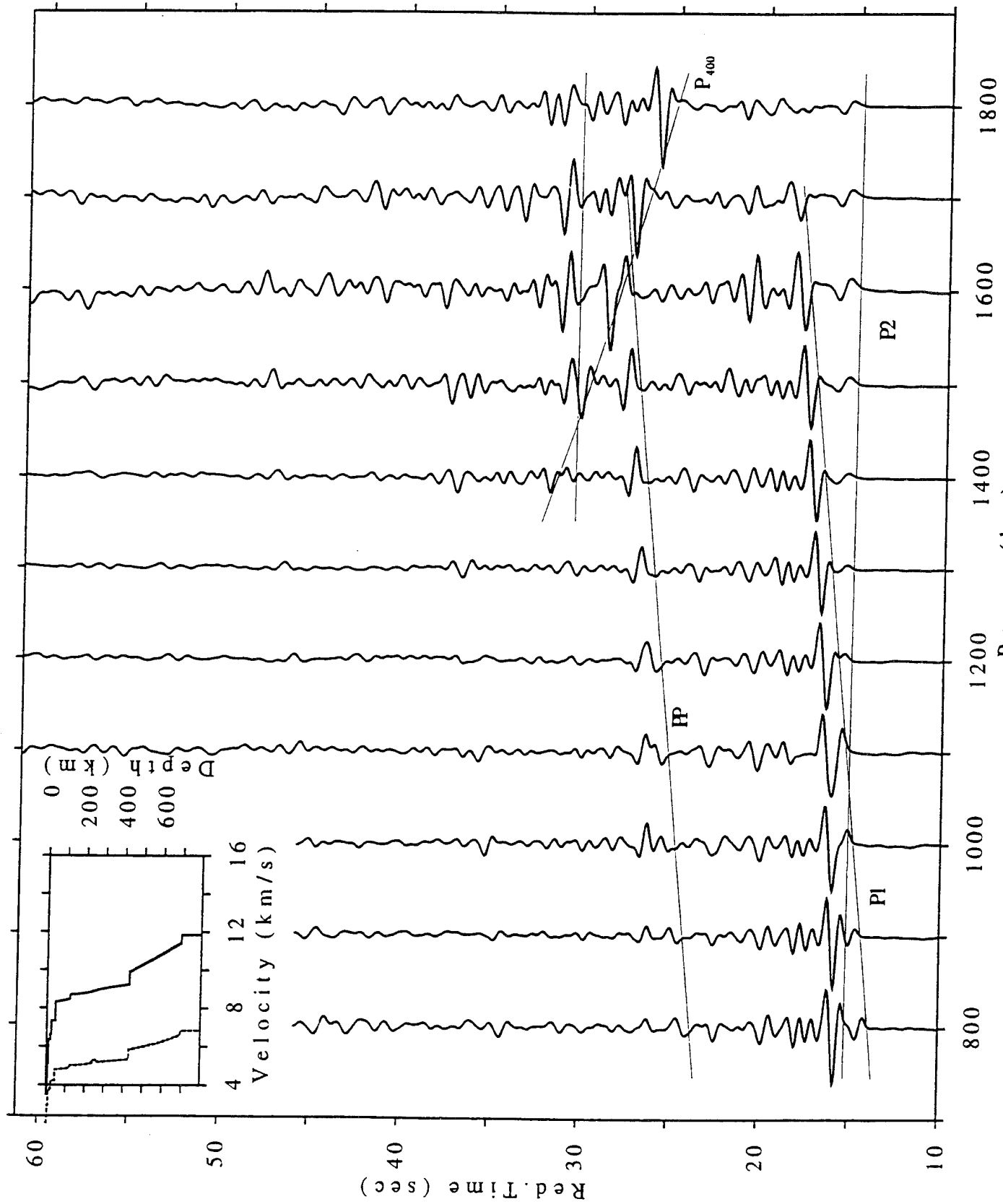


Figure 8b

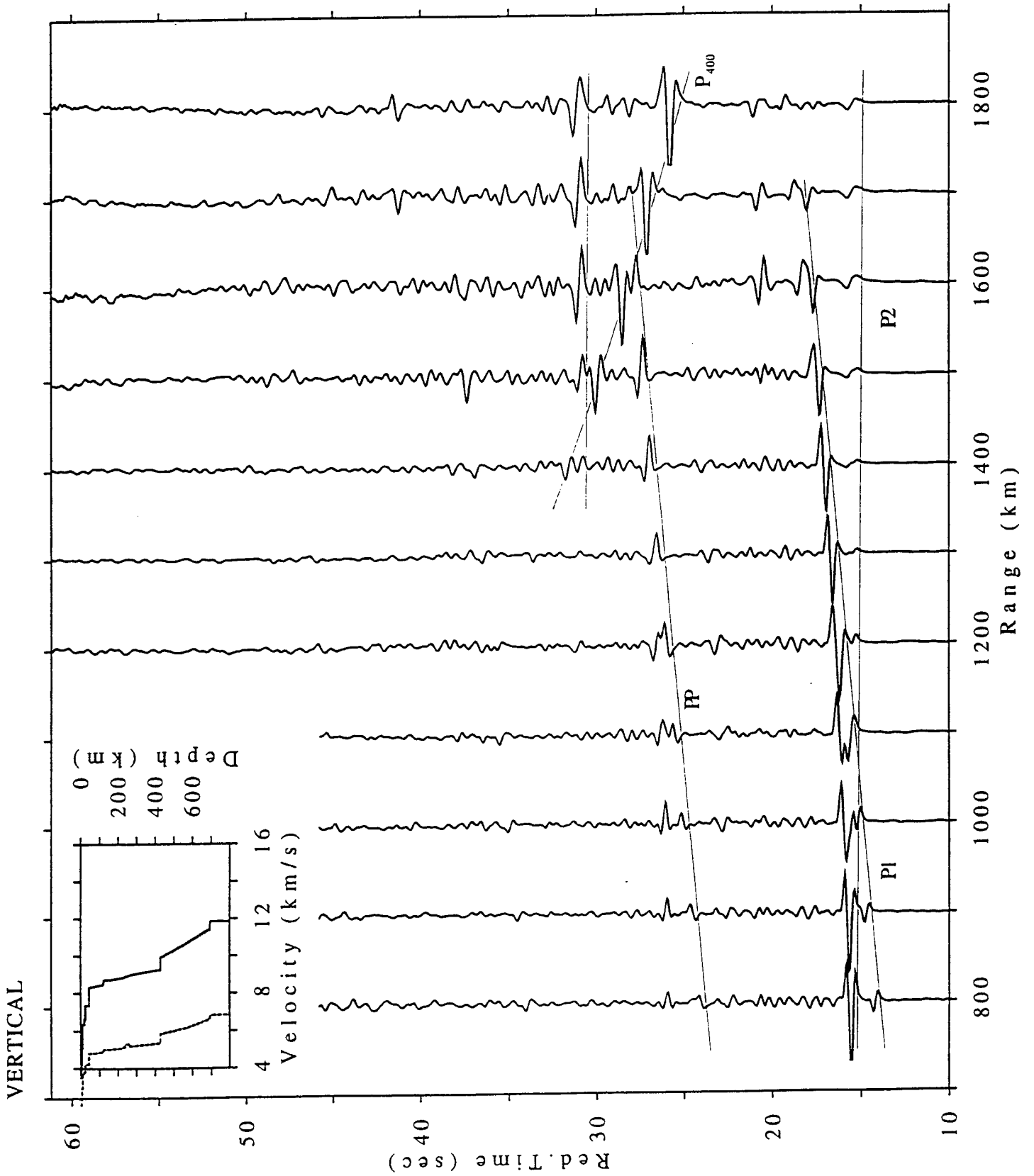
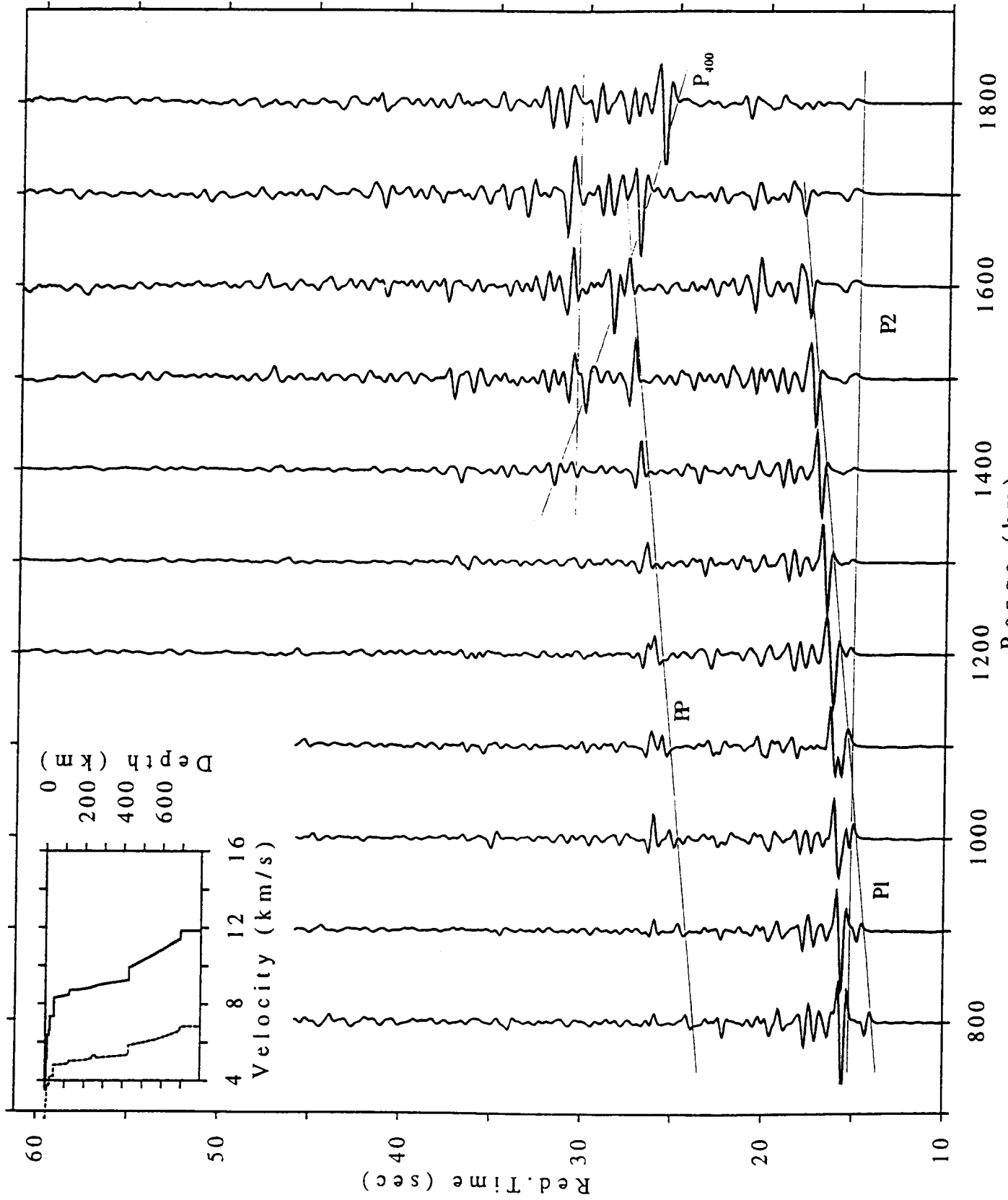
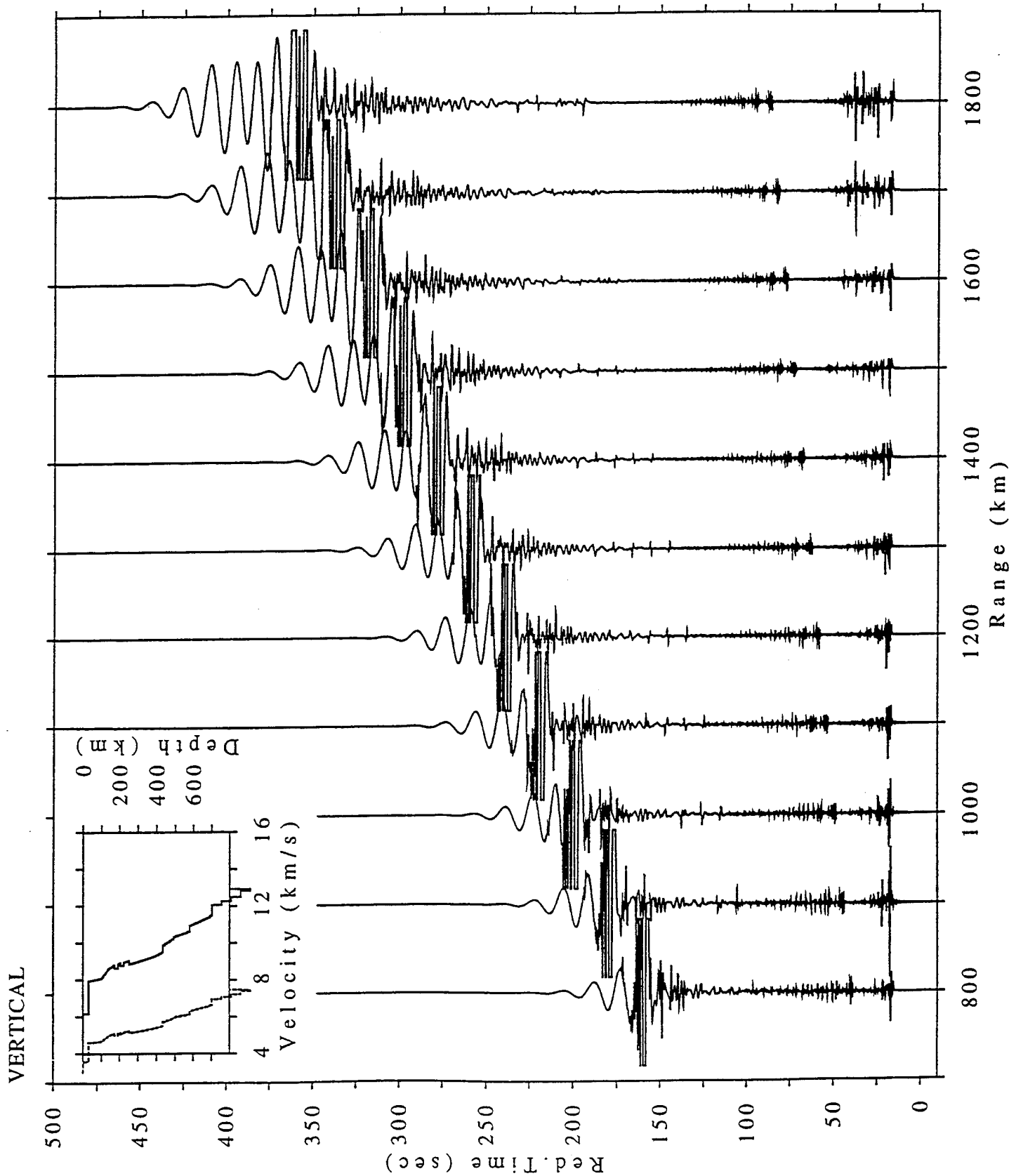


Figure 9: Synthetic seismograms as in Fig.8 but for a source duration of 0.5 sec (reduction velocity: 8.7km/sec).

HORIZONTAL



Range (km)  
Figure 9b



**Figure 10.** Complete synthetic seismograms for two P wave models used in Fig. 7. The S wave structure was constrained to Poisson's ratio of 0.25. Reduction velocity used was 8.7 km/sec.

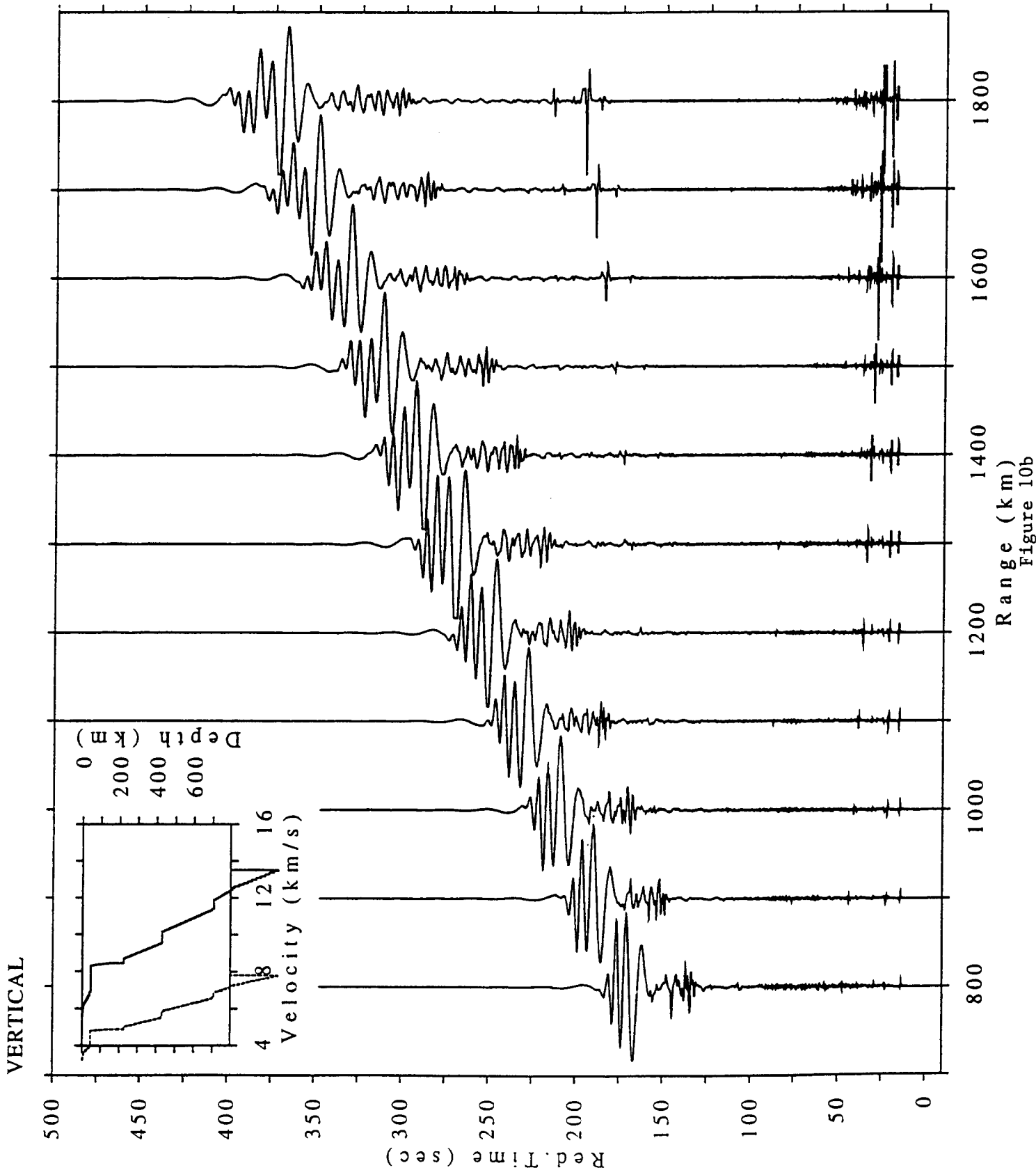


Figure 10b

Prof. Thomas Ahrens  
Seismological Lab, 252-21  
Division of Geological & Planetary Sciences  
California Institute of Technology  
Pasadena, CA 91125

Prof. Keiiti Aki  
Center for Earth Sciences  
University of Southern California  
University Park  
Los Angeles, CA 90089-0741

Prof. Shelton Alexander  
Geosciences Department  
403 Deike Building  
The Pennsylvania State University  
University Park, PA 16802

Dr. Thomas C. Bache, Jr.  
Science Applications Int'l Corp.  
10260 Campus Point Drive  
San Diego, CA 92121 (2 copies)

Prof. Muawia Barazangi  
Cornell University  
Institute for the Study of the Continent  
3126 SNEE Hall  
Ithaca, NY 14853

Dr. Douglas R. Baumgardt  
ENSCO, Inc  
5400 Port Royal Road  
Springfield, VA 22151-2388

Dr. T.J. Bennett  
S-CUBED  
A Division of Maxwell Laboratories  
11800 Sunrise Valley Drive, Suite 1212  
Reston, VA 22091

Dr. Robert Blandford  
AFTAC/TT, Center for Seismic Studies  
1300 North 17th Street  
Suite 1450  
Arlington, VA 22209-2308

Dr. Steven Bratt  
ARPA/NMRO  
3701 North Fairfax Drive  
Arlington, VA 22203-1714

Dale Breeding  
U.S. Department of Energy  
Recipient, IS-20, GA-033  
Office of Arms Control  
Washington, DC 20585

Dr. Jerry Carter  
Center for Seismic Studies  
1300 North 17th Street  
Suite 1450  
Arlington, VA 22209-2308

Mr Robert Cockerham  
Arms Control & Disarmament Agency  
320 21st Street North West  
Room 5741  
Washington, DC 20451,

Dr. Zoltan Der  
ENSCO, Inc.  
5400 Port Royal Road  
Springfield, VA 22151-2388

Dr. Stanley K. Dickinson  
AFOSR/NM  
110 Duncan Avenue  
Suite B115  
Bolling AFB, DC

Dr Petr Firbas  
Institute of Physics of the Earth  
Masaryk University Brno  
Jecna 29a  
612 46 Brno, Czech Republic

Dr. Mark D. Fisk  
Mission Research Corporation  
735 State Street  
P.O. Drawer 719  
Santa Barbara, CA 93102

Dr. Cliff Frolich  
Institute of Geophysics  
8701 North Mopac  
Austin, TX 78759

Dr. Holly Given  
IGPP, A-025  
Scripps Institute of Oceanography  
University of California, San Diego  
La Jolla, CA 92093

Dr. Jeffrey W. Given  
SAIC  
10260 Campus Point Drive  
San Diego, CA 92121



Dan N. Hagedorn  
Pacific Northwest Laboratories  
Battelle Boulevard  
Richland, WA 99352

Robert C. Kemerait  
ENSCO, Inc.  
445 Pineda Court  
Melbourne, FL 32940

Dr. James Hannon  
Lawrence Livermore National Laboratory  
P.O. Box 808, L-205  
Livermore, CA 94550

U.S. Dept of Energy  
Max Koontz, NN-20, GA-033  
Office of Research and Develop.  
1000 Independence Avenue  
Washington, DC 20585

Dr. Roger Hansen  
University of Colorado, JSPC  
Campus Box 583  
Boulder, CO 80309

Dr. Richard LaCoss  
MIT Lincoln Laboratory, M-200B  
P.O. Box 73  
Lexington, MA 02173-0073

Prof. Charles A. Langston  
Geosciences Department  
403 Deike Building  
The Pennsylvania State University  
University Park, PA 16802

Prof. Danny Harvey  
University of Colorado, JSPC  
Campus Box 583  
Boulder, CO 80309

Jim Lawson, Chief Geophysicist  
Oklahoma Geological Survey  
Oklahoma Geophysical Observatory  
P.O. Box 8  
Leonard, OK 74043-0008

Prof. Donald V. Helmberger  
Division of Geological & Planetary Sciences  
California Institute of Technology  
Pasadena, CA 91125

Prof. Thorne Lay  
Institute of Tectonics  
Earth Science Board  
University of California, Santa Cruz  
Santa Cruz, CA 95064

Prof. Eugene Herrin  
Geophysical Laboratory  
Southern Methodist University  
Dallas, TX 75275

Dr. William Leith  
U.S. Geological Survey  
Mail Stop 928  
Reston, VA 22092

Prof. Robert B. Herrmann  
Department of Earth & Atmospheric Sciences  
St. Louis University  
St. Louis, MO 63156

Mr. James F. Lewkowicz  
Phillips Laboratory/GPE  
29 Randolph Road  
Hanscom AFB, MA 01731-3010( 2 copies)

Prof. Lane R. Johnson  
Seismographic Station  
University of California  
Berkeley, CA 94720

Dr. Gary McCartor  
Department of Physics  
Southern Methodist University  
Dallas, TX 75275

Prof. Thomas H. Jordan  
Department of Earth, Atmospheric &  
Planetary Sciences  
Massachusetts Institute of Technology  
Cambridge, MA 02139

Prof. Thomas V. McEvilly  
Seismographic Station  
University of California  
Berkeley, CA 94720

Dr. Keith L. McLaughlin  
S-CUBED  
A Division of Maxwell Laboratory  
P.O. Box 1620  
La Jolla, CA 92038-1620

Prof. Bernard Minster  
IGPP, A-025  
Scripps Institute of Oceanography  
University of California, San Diego  
La Jolla, CA 92093

Prof. Brian J. Mitchell  
Department of Earth & Atmospheric Sciences  
St. Louis University  
St. Louis, MO 63156

Mr. Jack Murphy  
S-CUBED  
A Division of Maxwell Laboratory  
11800 Sunrise Valley Drive, Suite 1212  
Reston, VA 22091 (2 Copies)

Dr. Keith K. Nakanishi  
Lawrence Livermore National Laboratory  
L-025  
P.O. Box 808  
Livermore, CA 94550

Prof. John A. Orcutt  
IGPP, A-025  
Scripps Institute of Oceanography  
University of California, San Diego  
La Jolla, CA 92093

Dr. Howard Patton  
Lawrence Livermore National Laboratory  
L-025  
P.O. Box 808  
Livermore, CA 94550

Dr. Frank Pilotte  
HQ AFTAC/TT  
1030 South Highway A1A  
Patrick AFB, FL 32925-3002

Dr. Jay J. Pulli  
Radix Systems, Inc.  
6 Taft Court  
Rockville, MD 20850

Prof. Paul G. Richards  
Lamont-Doherty Earth Observatory  
of Columbia University  
Palisades, NY 10964

Mr. Wilmer Rivers  
Multimax Inc.  
1441 McCormick Drive  
Landover, MD 20785

Dr. Alan S. Ryall, Jr.  
Lawrence Livermore National Laboratory  
L-025  
P.O. Box 808  
Livermore, CA 94550

Dr. Chandan K. Saikia  
Woodward Clyde- Consultants  
566 El Dorado Street  
Pasadena, CA 91101

Mr. Dogan Seber  
Cornell University  
Inst. for the Study of the Continent  
3130 SNEE Hall  
Ithaca, NY 14853-1504

Secretary of the Air Force  
(SAFRD)  
Washington, DC 20330

Office of the Secretary of Defense  
DDR&E  
Washington, DC 20330

Thomas J. Sereno, Jr.  
Science Application Int'l Corp.  
10260 Campus Point Drive  
San Diego, CA 92121

Dr. Michael Shore  
Defense Nuclear Agency/SPSS  
6801 Telegraph Road  
Alexandria, VA 22310

Prof. David G. Simpson  
IRIS, Inc.  
1616 North Fort Myer Drive  
Suite 1050  
Arlington, VA 22209

Dr. Jeffrey Stevens  
S-CUBED  
A Division of Maxwell Laboratory  
P.O. Box 1620  
La Jolla, CA 92038-1620

Prof. Brian Stump  
Los Alamos National Laboratory  
EES-3  
Mail Stop C-335  
Los Alamos, NM 87545

TACTEC  
Battelle Memorial Institute  
505 King Avenue  
Columbus, OH 43201 (Final Report)

Prof. Tuncay Taymaz  
Istanbul Technical University  
Dept. of Geophysical Engineering  
Mining Faculty  
Maslak-80626, Istanbul Turkey

Phillips Laboratory  
ATTN: GPE  
29 Randolph Road  
Hanscom AFB, MA 01731-3010

Prof. M. Nafi Toksoz  
Earth Resources Lab  
Massachusetts Institute of Technology  
42 Carleton Street  
Cambridge, MA 02142

Phillips Laboratory  
ATTN: TSML  
5 Wright Street  
Hanscom AFB, MA 01731-3004

Dr. Larry Turnbull  
CIA-OSWR/NED  
Washington, DC 20505

Phillips Laboratory  
ATTN: PL/SUL  
3550 Aberdeen Ave SE  
Kirtland, NM 87117-5776 (2 copies)

Dr. Karl Veith  
EG&G  
5211 Auth Road  
Suite 240  
Suitland, MD 20746

Dr. Michel Campillo  
Observatoire de Grenoble  
I.R.I.G.M.-B.P. 53  
38041 Grenoble, FRANCE

Prof. Terry C. Wallace  
Department of Geosciences  
Building #77  
University of Arizona  
Tuscon, AZ 85721

Dr. William Wortman  
Mission Research Corporation  
8560 Cinderbed Road  
Suite 700  
Newington, VA 22122

Prof. Hans-Peter Harjes  
Institute for Geophysics  
Ruhr University/Bochum  
P.O. Box 102148  
4630 Bochum 1, GERMANY

ARPA, OASB/Library  
3701 North Fairfax Drive  
Arlington, VA 22203-1714

Prof. Eystein Husebye  
IFJF  
Jordskjelvstasjonen  
Allegaten 41, 5007 BERGEN NORWAY

HQ DNA  
ATTN: Technical Library  
Washington, DC 20305

David Jepsen  
Acting Head, Nuclear Monitoring Section  
Bureau of Mineral Resources  
Geology and Geophysics  
G.P.O. Box 378, Canberra, AUSTRALIA

Defense Technical Information Center  
Cameron Station  
Alexandria, VA 22314 (2 Copies)

Ms. Eva Johannisson  
Senior Research Officer  
FOA  
S-172 90 Sundbyberg, SWEDEN

Dr. Peter Marshall  
Procurement Executive  
Ministry of Defense  
Blacknest, Brimpton  
Reading FG7-FRS, UNITED KINGDOM

Dr. Bernard Massinon, Dr. Pierre Mechler  
Societe Radiomana  
27 rue Claude Bernard  
75005 Paris, FRANCE (2 Copies)

Dr. Svein Mykkeltveit  
NTNT/NORSAR  
P.O. Box 51  
N-2007 Kjeller, NORWAY (3 Copies)

Dr. Jorg Schlittenhardt  
Federal Institute for Geosciences & Nat'l Res.  
Postfach 510153  
D-30631 Hannover , GERMANY

Dr. Johannes Schweitzer  
Institute of Geophysics  
Ruhr University/Bochum  
P.O. Box 1102148  
4360 Bochum 1, GERMANY

Trust & Verify  
VERTIC  
Carrara House  
20 Embankment Place  
London WC2N 6NN, ENGLAND